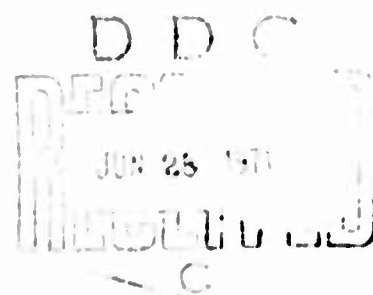# USAAVLABS TECHNICAL REPORT 71-12

# MODEL STUDIES OF HELICOPTER TAIL ROTOR FLOW PATTERNS IN AND OUT OF GROUND EFFECT

By

August F. Lehman

April 1971

# EUSTIS DIRECTORATE

# U. S. ARMY AIR MOBILITY RESEARCH AND DEVELOPMENT LABORATORY FORT EUSTIS, VIRGINIA

## DISCLAIMERS

## DISPOSITION INSTRUCTIONS

## DOCUMENT CONTROL DATA - R & D

*(Security classification of title, body of abstract and indexing annotation must be entered when the overall report is classified)*

| 1 ORIGINATING ACTIVITY *(Corporate author)* | 2a. REPORT SECURITY CLASSIFICATION |
|---|---|
| Oceanics, Inc.<br>Technical Industrial Park<br>Plainview, New York | Unclassified |
| | 2b. GROUP |

**3 REPORT TITLE**

MODEL STUDIES OF HELICOPTER TAIL ROTOR FLOW PATTERNS IN AND OUT OF GROUND EFFECT

**4 DESCRIPTIVE NOTES** *(Type of report and inclusive dates)*

Final Technical Report

**5 AUTHOR(S)** *(First name, middle initial, last name)*

August F. Lehman

| 6 REPORT DATE | 7a. TOTAL NO. OF PAGES | 7b. NO. OF REFS |
|---|---|---|
| April 1971 | 88 | 13 |

| 8a. CONTRACT OR GRANT NO. | 9a. ORIGINATOR'S REPORT NUMBER(S) |
|---|---|
| DAAJ02-68-C-0069 & DAAJ02-68-C-0103 | USAAVLABS Technical Report 71-12 |
| b. PROJECT NO.<br>Task 1F162204A14232 and | |
| c.     1F162204A14231 | 9b. OTHER REPORT NO(S) *(Any other numbers that may be assigned this report)*<br>70-79 |
| d. | |

**10. DISTRIBUTION STATEMENT**

Approved for public release; distribution unlimited.

| 11. SUPPLEMENTARY NOTES | 12. SPONSORING MILITARY ACTIVITY |
|---|---|
| | Eustis Directorate, U. S. Army Air<br>Mobility Research and Development<br>Laboratory, Fort Eustis, Virginia |

**13. ABSTRACT**

Water tunnel studies of a model helicopter which entailed a
visualization of the main and tail rotor wakes, the inflow
patterns, and their subsequent interactions as the wind
velocity and wind heading were changed resulted in a
significant gain in knowledge ultimately applicable to
direction control of helicopters.  Of significant interest
was the impingement of the main rotor wake with a ground
plane, its subsequent spreading outward in a radial manner
and the roll-up of the wake into a standing vortex at the
outer edge of this radial expansion of the wake.  The position
of the rolled-up vortex on the ground plane, with reference
to the flow field in and about the tail rotor, plays a
dominant role in determining the resultant velocity vectors
relative to the tail rotor blades (and consequently the
tail rotor's thrust and torque characteristics).  The
ingestion of the tail rotor wake by the main rotor and the
annulus nature of the tail rotor wake are factors which
perhaps deserve more attention, in terms of understanding
helicopter directional control, than they have received in
the past.

**DD** FORM **1473** REPLACES DD FORM 1473, 1 JAN 64, WHICH IS OBSOLETE FOR ARMY USE.

| 14. KEY WORDS | LINK A | | LINK B | | LINK C | |
|---|---|---|---|---|---|---|
| | ROLE | WT | ROLE | WT | ROLE | WT |
| Flow Visualization | | | | | | |
| Helicopter Rotor | | | | | | |
| Rotor Flow Patterns | | | | | | |
| Aerodynamics | | | | | | |
| Water Tunnel Tests | | | | | | |

This report has been reviewed by the Eustis Directorate, U.S. Army Air Mobility Research and Development Laboratory, and is considered to be technically sound. The purpose of this investigation was to visually record and study the main and tail rotor vortex patterns in and out of ground effect while varying parameters such as wind azimuth and velocity, main rotor disc loading, jet engine exhaust, and tail rotor location (pusher or tractor).

The investigation was conducted under the technical management of Mr. William Sickles, Mr. John Shipley, Mr. William Yeager, and Mr. Patrick Cancro of the Aeromechanics Division of this Directorate.

Tasks 1F162204A14232
1F162204A14231

Contracts DAAJ02-68-C-0069
DAAJ02-68-C-0103
USAAVLABS Technical Report 71-12
April 1971

MODEL STUDIES OF HELICOPTER
TAIL ROTOR FLOW PATTERNS
IN AND OUT OF GROUND EFFECT

Oceanics Report No. 70-79

Details of illustrations in
this document may be better
studied on microfiche.

by
August F. Lehman

Prepared by

Oceanics, Inc.
Plainview, New York

for

EUSTIS DIRECTORATE
U. S. ARMY AIR MOBILITY RESEARCH AND DEVELOPMENT LABORATORY
FORT EUSTIS, VIRGINIA

# ABSTRACT

Water tunnel studies of a model helicopter which entailed a visualization of the main and tail rotor wakes, the inflow patterns, and their subsequent interactions as the wind velocity and wind heading were changed resulted in a significant gain in knowledge ultimately applicable to directional control of helicopters.  Of significant interest was the impingement of the main rotor wake with a ground plane, its subsequent spreading outward in a radial manner, and the roll-up of the wake into a standing vortex at the outer edge of this radial expansion of the wake.  The position of the rolled-up vortex on the ground plane, with reference to the flow field in and about the tail rotor, plays a dominant role in determining the resultant velocity vectors relative to the tail rotor blades (and consequently the tail rotor's thrust and torque characteristics).  The ingestion of the tail rotor wake by the main rotor and the annulus nature of the tail rotor wake are factors which perhaps deserve more attention, in terms of understanding helicopter directional control, than they have received in the past.

# FOREWORD

# CONTENTS

# LIST OF ILLUSTRATIONS

## INTRODUCTION

The inability to reasonably predict, understand, or alleviate tail-rotor/tail-boom/main-rotor influence on performance has resulted in helicopters with inadequate or marginal directional control. In an attempt to better understand the phenomenon involved, a program involving model studies in a water tunnel was performed since water tunnel test procedures offered certain advantages over conventional wind tunnel test procedures. In particular, water tunnel testing permits simultaneous observation of the tip vortex trails associated with both the main and tail rotors and an observation of the inflow streampaths to either rotor. Also, the differences in the kinematic and dynamic viscosities between water and air offer additional advantages for the use of water when scale models are being tested. These advantages will be discussed in detail in later sections of this report.

The general objective of the program concerned a visualization of main and tail rotor tip vortex patterns in and out of ground effect and the inflow streampaths to the tail rotor. More specifically, wind azimuth and velocity, main rotor disc loading, jet engine exhaust, and tail rotor location, i.e., pusher or tractor configuration, were parameters subject to variation. Each of the test configurations was observed visually and documented with high-speed movies and still photography.

## TECHNICAL APPROACH TO THE PROBLEM

In establishing the test program there were two major considerations requiring close attention. The first involved a determination that the proposed tests simulated, in a reasonable manner, conditions existing in the operational environment of the full-scale prototype. The second consideration involved the techniques which permitted an observation of the rotors' tip vortex trails (or their wakes) and the streampath inflow patterns.

Discussion of the second consideration may be disposed of in a somewhat less involved manner than the first; therefore, that discussion will be presented first, although in practice, a determination of the scaling factors is the primary consideration because the test results are of dubious value if appropriate scaling is not achieved.

## OBSERVATION OF FLOW PATTERNS

The flow patterns or wakes created by an object in incompressible airflows will also be created by the object if water rather than air is the test medium. If observations of vortex patterns are of interest, water as the test medium has a preference to air since air bubbles bled into the vortex region will be centrifuged to the center or core of the vortex. This occurs because of the lesser density of the air bubbles in comparison to the density of water and the rotational motion of the fluid in the vortex. In this manner, the core of the vortex is made easily visible and the location of the core can be documented with regular or high-speed movies, or with still photography.

The air bubbles which depict the core of the vortex cannot distort the core location since the air bubbles can exert no influence on the physical phenomenon which produced the vortex. Also, the bubbles cannot depict a "false core" location since, upon leaving the vortex core or center, the bubbles become widely disbursed through the fluid rotating about the vortex core. Thus the bubbles no longer indicate any well defined or easily discernible core path. Because of this latter characteristic, the amount of air bled into the vortex is somewhat critical if observations of the vortex flow are not to be "muddied" by many free air bubbles in the surrounding field of observation.

The use of the air bubble technique to define the location of vortex cores in water tunnel studies has an advantage over the use of neutral density dye injection (which compares

2

to smoke injection in wind tunnel investigations) because
air bubble injection need only take place near the vortex
formation as the lesser density of the air bubbles, coupled
with the rotation of the vortex, centrifuges the air to the
center of the vortex.  In contrast, dye streaks can follow
the streampath only from the point of dye injection, and
if the dye injection point is not located on the stream-
path which eventually enters into the vortex core, the dye
streak cannot locate the vortex core; it can only depict
some element of fluid in the overall vorticity field.

Neutral density dye streak techniques are of value in water
tunnel studies just as smoke techniques are of value in
wind tunnel studies when inflow patterns are of interest.
Therefore, this study employed the air bubble technique for
a determination of the tip vortex patterns and the neutral
density dye injection technique for the observation of
inflow patterns.  In the photographs which illustrate the
tip vortex and inflow patterns an arrow indicates the free
stream velocity direction.


## MODEL/FULL-SCALE SIMILITUDE

In order for test results involving reduced scale models to
be of value, certain parameters must be scaled in accordance
with established dimensional analysis procedures.  In this
study it was believed that four characteristics had to be
appropriately scaled:  model geometry, main rotor lift, jet
engine exhaust, and a new characteristic, believed to be
important in tunnel studies of models having sharply
deflected wakes, identified here as the wake energy
dissipation pattern and discussed in a section on page 6.


### Model Geometry

Geometric similarity was achieved by a linear scaling of
the prototype dimensions.  The prototype was the Bell AH-1G
(Cobra).  The airfoil profile, twist and precone angle of
the model main and tail rotors duplicated the prototype
exactly.  The model rotors were rigid; thus dynamic (mass
distribution and rotor attachment) similarity with the
prototype rotor was not achieved.  However, since this
study involved total rotor lift and the interaction of the
tip vortex wake patterns of the main and tail rotor, it
was believed that complete dynamic similarity was not
necessary.  It is recognized that with investigations
involving main rotor lift fluctuations as a function of
rotor azimuth position, rotor blade slap, or similar
phenomena, dynamic similarity may become a required scaling

3

factor.

## Rotor Lift

The attainment of appropriate rotor lift similarity involves
consideration of the Reynolds number, the incompressible-
compressible data correction, and the rotor advance ratio.

### Reynolds Number Effect

The degree of matching of the model and full-scale
Reynolds number is always of concern, particularly so
when testing lifting models.  This concern is related
to the fact that while the basic slope of the lift
coefficient-section attack angle curve may not be
significantly altered with a change in Reynolds number,
the maximum lift coefficient which can be obtained
before the initiation of stall is strongly dependent
on Reynolds number.

The prototype Reynolds number, derived from the rotor
chord length and for a tip velocity of 800 feet per
second, is of the order of $10.3 \times 10^6$.  For the water
tunnel tests, while the model rotor is quite small, the
difference in the kinematic viscosity between air and
water is advantageous, resulting in a model Reynolds
number of the order of $1.7 \times 10^5$.  Thus, there is a
difference in the magnitude of the full-scale and model
Reynolds numbers.  However, the matter of concern when
the lift and wake characteristics of a rotor are of
interest lies primarily in the maximum lift coefficient
obtainable (as a function of radial location) before
stall occurs.  In the case of rotor studies, the section
angle of attack and Reynolds number at different radial
stations must be examined to determine the difference in
lift characteristics existing at specific radial stations
of a rotor when operating at two different Reynolds
numbers (model and full-scale).

In Appendix I, such a comparison calculation is made for
a rotor operating at Reynolds numbers comparable to the
full-scale and model values of this study.  That com-
parison shows that on the basis just described, the
calculated difference in the rotor loading at two
Reynolds numbers is of the order of 1 percent (for the
hover case) at a prototype rotor collective pitch angle
corresponding to a load of 8,000 pounds.  In other words,
the calculated lift performance of a rotor operating at
the full-scale and the model Reynolds numbers is

4

remarkably close when considering only Reynolds number influence.

## Compressible Vs. Incompressible Test Data

The full-scale rotor was assumed to have a constant tip velocity of 800 feet per second; thus compressibility effects will influence its performance. On the other hand, the model rotor is operating in water; therefore, its operating regime is fully incompressible. A reasonable approximation for estimating the compressibility effects on incompressible data (when the lifting surface is not in a stall condition) is to employ the Prandtl-Glauert factor, which is $\sqrt{1-M_\infty^2}$. Payne, in Reference 1, shows that the thrust coefficient obtained with an incompressible (nonstalling flow situation, divided by the Prandtl-Glauert factor, provides good agreement with compressible flow thrust coefficient data. The Mach number (M) is taken as that occurring at the 0.7 radial section of the rotor.

## Rotor Advance Ratio

To insure appropriate scaling of rotor operation with forward velocity, the advance ratio ($\mu$), defined as the free-stream velocity divided by the rotor tip speed velocity, was determined from full-scale operational values. It was then employed to determine the free-stream velocity required in the tunnel for a constant model main rotor tip speed of 29.31 feet per second.

## Jet Engine Exhaust

One aspect of this program concerned the influence of jet engine exhaust on the tail rotor wake. Therefore, a valid scaling of the prototype jet engine exhaust was necessary. In the model, the jet engine exhaust was simulated by a water jet since water was the test medium representing the air in prototype operation. Several different factors for exhaust scaling were developed, and these scaling factors resulted in remarkably close agreement with each other when used to determine the model jet exhaust velocity. Appendix II presents details of the scaling factor selected for use in this study. This factor kept, as a constant, the ratio of the jet engine exhaust momentum to the tail rotor thrust; i.e.,

$$\frac{\text{Total momentum of the jet engine exhaust}}{\text{Tail rotor thrust}} = \text{Constant}$$

5

## Wake Energy Dissipation Pattern

Reference 2 concerned the initial studies of a model
helicopter rotor in a water tunnel. That study involved
a 12-inch-diameter model of a 48-foot-diameter Bell HU-1D
rotor. The same geometric scaling factors described in
this report were employed in the construction of that
rotor. The tests were performed in a 20-inch by 20-inch
cross-sectional test section. The excellent agreement
between model lift coefficient-rotor collective pitch
angle data when compared with the full-scale values was
difficult to understand in view of the theoretical
studies of References 3, 4, and 5 and the wind tunnel
studies of References 6 and 7, which indicated that
relatively large test sections are required if sharply
deflected wakes are being investigated. Therefore, in an
effort to determine the cause for this apparent variation
in water and wind tunnel test section size requirements
when studying sharply deflected wakes, a study of the
effect of tunnel test section size on rotor lift and wake
characteristics when water was the test medium was
performed.

That study, Reference 8, revealed that because a real
fluid is involved, both the kinematic viscosity of the
fluid (which is associated with the Reynolds number) and
the dynamic viscosity of the fluid (which is a measure of
the shear stress or energy absorption characteristic of
the fluid) must be considered if appropriate wake scaling
is to be achieved between the model and prototype.

The situation can be considered as one wherein the rotor is
injecting energy into the fluid stream, which is then being
absorbed by the viscous action of the surrounding fluid. It
is believed that the wake energy dissipation pattern,
created by the model in the model test medium, must scale
the wake energy dissipation pattern created by the full-
scale vehicle when in its operating medium if similar wake
patterns are to be achieved. From this it follows that
when considering tunnel test section size influence on the
rotor performance, rotor lift coefficient agreement is not
sufficient. The absolute rotor load and the viscosity of
the fluid in which the rotor operates should be considered.
The importance of the absolute load when testing aircraft
models with sharply deflected wakes was recognized by
South in Reference 9 but was not carried to the conclusion
of including the equally important aspect of fluid
viscosity, probably because wind tunnel studies do not
entail significant differences in the model test fluid
viscosity compared with the viscosity in which the
prototype operates. Thus this inability to vary the model

test fluid viscosity may be considered a disadvantage when considering the proper scaling of model studies performed in air with model studies performed in a more viscous fluid such as water.

As an example of the importance of scaling the wake energy dissipation pattern, consider a full-scale hovering rotor operating in air with a rotor disc load of 4 pounds per square foot. Under these conditions, the wake will be projected away from the rotor tip path plane some finite distance. As a first approximation, the distance the wake will be projected away from the rotor tip path plane is solely a function of the rotor disc load per unit area, not the absolute size of the rotor disc area, just as the projection distance of a jet from a nozzle is a function of nozzle pressure and not the absolute nozzle size. From this it follows that if the wake projection distance of a full-scale helicopter rotor (in hover) is defined as that clearance distance above the ground associated with out-of-ground-effect operation, the same clearance distance will be required in the model tests if the same rotor load per unit area is involved. From this it can be concluded that wind tunnel studies of rotors in the hover and transitional flight regimes will require large test sections because appropriate scaling of the Reynolds number will result in rotor disc loadings per unit area approaching those of the full-scale rotor and, as a consequence, the necessary large clearance distances before the presence of a boundary (floor, walls or ceiling) can be tolerated.

The wake energy dissipation pattern is directly related to the viscosity of the fluid in which the rotor is operating and the load per unit area of the rotor disc. If both the model and prototype rotors operate in the same medium, i.e., air, the wake dissipation pattern (or the wake projection distance) will be identical (as a first approximation) if the rotor load per unit area is the same for both the model and the full-scale vehicle. It has already been pointed out that appropriate Reynolds number scaling must be maintained between the model and the full-scale prototype, and it is this requirement which limits the degree of reduction that can be tolerated in the absolute rotor load per unit area when performing reduced scale model investigations.

To further illustrate the importance of maintaining wake energy dissipation similitude, consider the operation of a HU-1D helicopter in hover. Data for this aircraft indicates that it is out of ground effect at a clearance distance of the order of one rotor diameter or about 52 feet. From the preceding discussion, it follows that the

out-of-ground-effect distance will be affected by the
viscosity of the fluid as well as by the rotor load per
unit area. Considering a reduced scale model study of
this aircraft with a ground plane only, it again follows,
as a first approximation, that if the reduced scale model
rotor load per unit area were the same as for the full-
scale rotor, the ground clearance distance would also be
52 feet. In other words, if a 1/4 scale model were being
tested with the same rotor load per unit area as the
prototype, the data would indicate a clearance of 52
feet. This is a scaling ratio of clearance height to rotor
diameter of approximately 4 rather than the correct scaling
ratio of approximately 1. It is this inability to properly
match the wake characteristics in reduced scale model rotor
studies performed in air, while maintaining appropriate
Reynolds number scaling, that has led to the correct
conclusion by investigators of sharply deflected wakes that
relatively large wind tunnel test sections are required.

The matching of the model wake energy dissipation pattern
with the prototype was accomplished in these water tunnel
studies in the following manner. In Reference 8 a discussion
is presented of how the model rotor of a helicopter was
tested in the hover mode in the tunnel as a propeller, i.e.,
the axis of rotor rotation coincided with the longitudinal
axis of the test section. Through this approach, it was
possible to determine the absolute projection distance of
the wake when the rotor was operating at a rotational speed
sufficient to insure appropriate Reynolds number scaling.
With this operational condition, the wake projected from the
tip path plane a distance of approximately 1 model rotor
diameter. Therefore, the placement of a boundary at this
location should not influence the wake pattern, as no motion
of the flow field existed. The wake projection distance was
determined by placing tufts on fine cords which spanned the
test section on the vertical centerline. The movement of
the tufts indicated how far the wake energy projected into
the fluid stream before its axial motion was absorbed by the
water.

With a tunnel test section size of 28 inches by 28 inches
and a rotor diameter of 14 inches, it was therefore possible
to satisfy this clearance distance requirement of one rotor
diameter by mounting the rotor in the center of the test
section. References 3, 4, and 5 have indicated that the
presence of the floor dominates the influence of tunnel
test section size on rotor performance. Therefore, it
follows that if a rotor positioned in the center of an
equal-sided tunnel maintains a clearance above the floor
such that the floor does not influence the rotor's
performance, it is reasonable to expect that the walls and

8

ceiling will not significantly influence rotor performance
either. Details of the testing procedures developed for
water tunnel studies of sharply deflected wakes are fully
described in Reference 8.

## MODEL-TUNNEL SIZE CONSIDERATION

The selection of the model rotor size for the tunnel test
section size available, i.e., an equal-sided 28-inch by
28-inch test section, was initially determined through the
procedures described above and in Reference 8, wherein it
was determined that scaling of the wake energy dissipation
pattern was satisfied. In this section it is sufficient
to repeat that the model rotor diameter was 14 inches and
that for the out-of-ground-effect studies the model was
mounted at the vertical center of the test section, thus
satisfying the clearance determined earlier. For the ground
effect studies, a false floor was installed beneath the
model to give the appropriate clearance.

# TEST FACILITIES AND EQUIPMENT

## TUNNEL

The tests were run in the Oceanics water tunnel. This
tunnel is a recirculating, closed-jet-type tunnel having
both the water velocity and the test section static
pressure as controllable variables. The cross section
of the basic test section is equal sided with a side
dimension of 28 inches. The section has corner fillets
with a 2.36-inch radius. The useable length of the test
section is approximately 12 feet. Viewing windows are
on all four sides of the test section, thus permitting
excellent observation of the model undergoing tests.
For this study, the out-of-ground-effect conditions were
examined in the basic section. For the in-ground-effect
studies, a Plexiglas panel was inserted into the basic
section. This panel spanned the test section and extended
the length of the section.

In the settling section, just ahead of the nozzle, there
are two honeycombs which improve the flow before the water
enters the nozzle and passes into the test section. The
upstream honeycomb is an egg-crate type consisting of
square elements 1.12 inches on a side and having a length
of 7 inches. The honeycomb nearest the test section is
also an egg-crate type with the individual square elements
having a side dimension of 0.96 inch and a length of 16
inches.

## MODEL

The model of the helicopter was a scaled version of the Bell
AH-1G (Cobra). The two-bladed main rotor had a diameter of
14 inches. An NACA 0012 airfoil formed the cross-sectional
profile of the model main rotor blades. The main rotor
blades had a uniform twist from the root to the tip of
0.454 degree per foot (full-scale value), and the blades
were set into the hub with a precone angle of 2 degrees
45 minutes. The chord length of a model main rotor blade
was 0.716 inch. The main rotor blades were fitted into
a hub which permitted pitch adjustments to each individual
blade. This method of blade-hub attachment does not
duplicate the prototype. As pointed out earlier, since the
model attachment is rigid, the blades are not permitted to
translate except for deflections due to bending loads
introduced during operation.

The tail rotor blades were also geometrically scaled versions
of the prototype blades. But here also the blades were

10

rigidly attached to a hub. The tail rotor had a diameter of 2.784 inches, and the chord length of an individual blade was 0.245 inch. The chord thickness was 0.0294 inch. Because of the small physical size of the tail rotor, a mechanism permitting a change in the pitch of the individual blades in the hub attachment was not practical. Therefore, five tail rotors were fabricated with blades having pitch settings of 11, 13, 15, 17 and 19 degrees. The tail rotor blades were untwisted. Photographs of the main and tail rotors are shown in Figure 1.

The model fuselage was a fairly accurate representation of the prototype, although the landing skids and other minor appendages were not included in the model as it was believed that detailed refinements of this type were not necessary in the model to produce a test configuration which would permit a realistic investigation of the problem under consideration. The main rotor drive shaft was directly connected to a gear-box contained in the fuselage. The tail rotor was driven from this gearbox by a flexible belt containing teeth molded into its surface. These teeth fitted gears forming a part of each tail rotor assembly and the gearbox. In this manner, the tail rotor speed was held to a precise ratio with that of the main rotor. Several views of the model are shown in Figure 2.

The test assembly which supported and powered the model consisted of a variable-speed electric motor, a drive shaft instrumented to permit lift measurements when the model was not attached to it, a pylon surrounding the drive shaft, and two support struts for the aft of the model. The entire assembly was fastened to a turntable located in the tunnel floor. In this manner changes could be made in model azimuth. The motor and drive shaft could be tilted both fore and aft and in the lateral direction. An overall view of the test arrangement outside of the tunnel is shown in Figure 3.

The lift of the rotor was sensed in the direction along the drive shaft by utilizing a balance inserted (as a coupling) between the motor and the drive shaft. The balance was calibrated using a rig which incorporated dead weights certified to National Bureau of Standards Tolerance Class C. The calibration was performed with the test assembly mounted in the tunnel, submerged in water, and with the drive shaft operating at the test rotational speed. In this manner, any influence of the bearings in the pylon support was accounted for during the calibration procedure. The output from the balance transducer assembly was fed into an X-Y plotter, permitting the pen deflection, as measured from the trace of the X-Y plot, to be associated with known weights. Calibration was performed before beginning each day's tests.

11

## TEST PROCEDURES

The initial phase of this study involved a determination of the collective pitch setting on the main rotor which would produce the desired (scaled) vertical lifts. This information was obtained through a series of tests with the (isolated) main rotor. A range of collective pitch settings was tested while the equivalent velocity was varied over the speed range from hover to 30 knots. This model lift data was obtained with longitudinal mast angles associated with the 6,000- and 8,000-pound vertical lift conditions of the full-scale vehicle and in conjunction with lateral mast angles of 1.3 and 2.75 degrees. The mast angle data employed in this study are presented in Tables I and II.

The measured model rotor lift values converted to equivalent full-scale values corresponding to full-scale operating conditions of 6,000-foot altitude with an air temperature of 90 degrees Fahrenheit are shown in Figure 4. These data curves were then used in selecting the model main rotor collective pitch values for each of the specified test conditions. The tail rotor collective pitch angles for each test condition were determined from the data presented in Tables III and IV. The obtaining of the proper simulated jet exhaust flow rates was established by performing a series of time-volume measurements for the model (water) jet exhaust as a function of feed water metering valve position.

Having now established all characteristic variables required for the different test conditions, each particular test situation was established in the tunnel and the wake and/or inflow patterns were documented through high-speed movies and still photography. Air was emitted from the tips of both main rotor blades when the tip vortex trail from the main rotor was the subject of interest. However, air was emitted from the tip of only one tail rotor blade since air emitted from both tips produced a tip vortex pattern which tended to "smear" the individual vortex trails together because of the small spacing between successive vortex trails.

12

| TABLE I. LONGITUDINAL MAST TILT ANGLES (DEG)* | | | | | |
|---|---|---|---|---|---|
| Weight (lb) | Velocity (kt) | | | | |
| | 0 | 10 | 15 | 20 | 30 |
| 9500 | -0.3 | -0.4 | -0.5 | -0.6 | -0.8 |
| 8000 | -1.5 | -1.7 | -1.85 | -2.0 | -2.3 |
| 6000 | -0.3 | -0.4 | -0.5 | -0.6 | -0.8 |

Linear interpolations between points are permitted.

*USAAVLABS data obtained from full-scale vehicle operational information.

| TABLE II. LATERAL MAST TILT ANGLES (DEG)* | | |
|---|---|---|
| Weight (lb) | Tail Rotor Pitch Settings (deg) | |
| | 11 | 19 |
| 9500 | 1.10 | 2.32 |
| 8000 | 1.29 | 2.75 |
| 6000 | 1.72 | 3.69 |

Linear interpolations between points are permitted.

*USAAVLABS data obtained from full-scale vehicle operational information.

13

| Wind Direction (deg) | Wind Velocity (kt) | | | | |
|---|---|---|---|---|---|
| | 0 | 10 | 15 | 20 | 30 |
| 0 | 11 | 13/13 | 17/17 | 17/17 | 19/17 |
| 45 | 11 | 14/13 | 16.3/15.6 | 16.2/15.7 | 13.7/15.8 |
| 90 | 11 | 14.8/13.1 | 15.8/14.2 | 15.4/14.15 | 15/15 |
| 135 | 13 | 15.9/13.1 | 13.7/12.5 | 13.5/12.8 | 15/15 |
| 165 | 13 | 16.7/13/25 | 12.3/11.3 | 12.3/11.5 | 13/13 |
| 180 | 15 | 17/13.25 | 13/10.9 | 11.7/11.15 | 12.5/11 |
| 195 | 15 | 19/16.2 | 15/10.4 | 11.4/10.3 | 12/11 |
| 210 | 17 | 19/15.1 | 17/13.6 | 12.2/10.45 | 12/11 |
| 225 | 15 | 19/14.1 | 15/9.3 | 11/8.25 | 11/11 |
| 240 | 13 | 17/13 | 14.2/12.8 | 11/9.3 | 11/11 |
| 275 | 11 | 15 | 12 | 11 | 11 |
| 315 | 11 | 13 | 11 | 11 | 11 |

**TABLE III. TAIL ROTOR PITCH SETTING, MAXIMUM AND MEAN ANGLE, PUSHER TAIL ROTOR CONFIGURATION, 8000 POUNDS GROSS WEIGHT***

For 9500 pounds gross weight, and 1 degree to maximum tail rotor settings contained inside of boxed area. All other values remain unchanged.

*USAAVLABS data obtained from full-scale vehicle operational information.

| Wind Direction (deg) | Wind Velocity (kt) | | | | |
|---|---|---|---|---|---|
| | 0 | 10 | 15 | 20 | 30 |
| 0 | 13/11 | 13/12.9 | 14.0/13.2 | 15 | 16 |
| 45 | 15 | 15.1/14.8 | 15.8/14.6 | 16 | 17 |
| 90 | 17 | 17.4/16.6 | 19/15.7 | 19 | 19 |
| 135 | 15 | 15.8/14.6 | 15.8/13.6 | 15 | 17 |
| 165 | 13 | 17/15.4 | 16.5/13.9 | 15 | 15 |
| 180 | 15 | 17.3/15.2 | 17.8/14.3 | 15 | 17/15 |
| 195 | 13 | 16.4/14.4 | 16.3/13.7 | 13.2 | 15 |
| 210 | 13 | 15.7/14.2 | 15.7/13.6 | 15.7/13 | 15.7/13 |
| 225 | 13 | 16.2/15.8 | 13/11.7 | 11 | 11 |
| 240 | 13 | 17.1/16.3 | 11/9.7 | 11 | 11 |
| 275 | 13 | 15.7/16.3 | 15.4/13.6 | 11 | 11 |
| 315 | 13 | 14.5/13.7 | 14.4/13.9 | 13 | 13 |

TABLE IV. TAIL ROTOR PITCH SETTING, MAXIMUM AND MEAN ANGLE, TRACTOR TAIL ROTOR CONFIGURATION, 8000 POUNDS GROSS WEIGHT*

For 9500 pounds gross weight, add 1 degree to maximum tail rotor settings contained inside of boxed area. All other values remain unchanged.

*USAAVLABS data obtained from full-scale vehicle operational information.

## TEST RESULTS - EVALUATION AND DISCUSSION

The data from this series of investigations consist of high-speed movie clips and still camera photographs. All of these data are at USAAVLABS.

Before discussing and evaluating the observations made during the test program, the conditions and assumptions employed in the test program will once again be reviewed.

1. Geometric similarity of rotor blade shape and fuselage outline was achieved by direct linear scaling.

2. Dynamic similarity of the rotor blade(s) was not achieved since it is believed that a study of the type discussed here does not require such detailed representation between the model and the prototype.

3. The physical size of the model main rotor and the test rotational speed was determined by comparing the calculated rotor lift (at hover) at the prototype and resulting model Reynolds number values and selecting the model size and model rotational speed corresponding to the calculated rotor lifts of a rotor operating at full-scale and model Reynolds number values differing by less than 2 percent.

4. The location of the model rotor in the test section was established as valid by matching the distance between the rotor and the floor with the wake energy dissipation pattern projection distance obtained at hover, when operating at the test speed obtained in 3 above.

5. The model main rotor collective pitch angles employed in this study were established through tests of the model rotor when operating as an isolated unit in the water tunnel. Corrections of these incompressible lift values to compressible values were made through the use of the Prandtl-Glauert factor by assuming a full-scale rotor tip speed of 800 feet per second and the Mach number existing at the 0.7 radial section of the full-scale main rotor blade.

16

6. The mast and fuselage orientation of the model was established by considering contributions from fore-and-aft cyclic, lateral cyclic, fuselage orientation, and the mast tilt of the prototype vehicle under operating conditions represented in the model test program.

7. Model jet engine exhaust similitude was established by maintaining, as a constant value, the total momentum of the jet engine exhaust divided by the tail rotor thrust, including corrections for density changes in the prototype jet engine exhaust.

8. The same ratio between prototype rotor tip speed and vehicle forward velocity was maintained in the model tests utilizing the model rotor tip speed which resulted in adequate Reynolds number scaling.

The flow field resulting from main-rotor/tail-rotor/tail-boom interaction on VTOL vehicles as the wind heading and velocity change is one of the most complex flow fields produced by any aircraft. Because of its complexity, perhaps a better insight into the ultimate flow situation can be gained if the individual components forming the ultimate flow field are initially reviewed by themselves. The major contributors to the flow field subject to individual review in this section are identified as follows:

1. Variations in the tail rotor inflow and wake as the wind heading and velocity are changed.

2. Interaction of the tail rotor inflow and wake with main rotor inflow and wake as the wind heading and velocity are changed.

3. Effect of the tail boom and tail fin on tail rotor inflow and wake, and possible changes in tail boom drag as the wind heading and velocity are changed.

4. Effect of a ground plane on the above three situations.

Before reviewing each of the above situations, the form of both rotor wakes will be briefly characterized. The blades of the main rotor are uniformly twisted from the root to the tip of the blade, with the higher relative attack angle at the root section. This change in section attack angle

17

of the blade, as a function of radial location, helps to
compensate for the variation in local section lift
resulting from the fact that the section rotational
velocity component is a function of the radial location.
By twisting the blade, the spanwise circulation
distribution of the main rotor is controlled so as to
obtain as much lift along the span as possible without
encountering local stall.

On the other hand, the blades of the tail rotor are not
twisted; therefore, the circulation distribution of the tail
rotor, ignoring the tip loss effect, is uniformly increasing
toward the tip.  On the basis of strip theory analysis, the
outer 20 percent of the tail rotor blade produces on the
order of 65 percent of the total lift (or thrust) of the
tail rotor.  As a consequence, the majority of the momentum
in the tail rotor wake is concentrated in the outer radii
locations of the tail rotor disc.  Thus the wake of the tail
rotor can be characterized as possessing an annular "jet"
form rather than a uniform "jet" form.  The annulus nature
of the tail rotor wake is believed to be a strong
contributory factor in the tail rotor wake's response to
the presence of the wind and/or the wake of the main rotor.

In the sections which follow, the comments have been arrived
at through deduction augmented by knowledge gained from this
and previous studies involving rotor wakes.  Later sections
will deal with specific test observations.


## VARIATIONS IN THE TAIL ROTOR INFLOW AND WAKE AS THE WIND
## HEADING AND VELOCITY ARE CHANGED

In analyzing this flow situation, consider an overhead view
of an isolated tail rotor, and mentally visualize the stream-
path flow patterns created by operating the tail rotor.  This
situation will be identified in further discussion as the
basic flow pattern.  The action of the wind on the basic
flow situation can be treated as a uniform $\Delta$-velocity
superimposed upon the streampath patterns visualized for the
basic flow situation.  It follows, therefore, that with a
wind heading of 90 degrees, that is, the wind impinging
(perpendicular) into the tail rotor disc, the $\Delta$-velocity
component associated with the wind reduces the effective
pitch setting of the rotor blade's airfoil sections.  For
this flow situation, an additional increment in the geometric
pitch setting of the tail rotor blade is required to produce
the same thrust as that which existed before the wind was
introduced.  It is interesting to observe that the torque
requirement related to the thrust produced should not be
changed for this wind heading situation.  The limiting factor

18

for this situation is related to the maximum geometric pitch setting to which the tail rotor can be set.

Consider now the situation wherein the wind is at a heading of 270 degrees. The superposition of the Δ-velocity component associated with the wind on the basic flow situation results in an alteration of both the inflow and wake streampath flow patterns. Recalling that a majority of the tail rotor momentum is concentrated near the tip sections of the tail rotor blade, it follows that the inflow streampaths near the tip of the rotor will be reversed, in direction, 180 degrees in order that flow can enter into the tail rotor disc area. Also, considering the flow on the downstream side of the tail rotor disc, the combination of the impinging wind against the tail rotor wake, coupled with the concentration of wake momentum in the outer locations of the tail rotor disc area, results in an expansion, mushrooming, or bellmouthing of the tail rotor wake such that the outer components of the wake, i.e., those components on its periphery, are influenced by the wind velocity vector so as to be swept past (upstream) the tip path plane of the tail rotor disc. However, upon progressing past the tip path plane, the fluid elements, which just were wake elements, are subject to the inflow demands of the rotor and are reingested by the tail rotor. Thus, under certain wind velocity magnitudes, a torus-like streampath pattern is established in and about the tail rotor tip region wherein the same fluid elements are being continuously reingested and expelled.

With the wind at either a 0 or a 180-degree heading, the combination of the wind Δ-velocity component super-imposed on the basic flow pattern situation produces a wake pattern which is identical for both cases. There is a skewing of both the inflow and the wake. Depending upon the magnitude of the wind velocity, the thrust and the torque requirements of the tail rotor will undergo change, the thrust being reduced and the torque being increased as the velocity increases. This occurs because the degree of skew distortion of the inflow and wake is directly related to the wind magnitude, and the inflow distortion is directly related to the thrust and torque characteristics of the rotor.

To summarize this section, then, it should be evident that the wind heading and velocity are not always detrimental to the tail rotor in terms of the torque required to produce a given amount of tail rotor thrust. This comment applies to an isolated tail rotor but holds for cases with or without a ground plane. With the wind at a 90-degree heading, the thrust and torque relationship should not be changed,

19

although the geometric pitch setting of the tail rotor to produce a given amount of thrust would differ. A deterioration in the amount of tail rotor thrust for a given torque input occurs when the heading of the wind is such as to influence both the inflow and wake. This situation would appear to exist for wind headings from about 190 to 290 degrees. The degree of deterioration in the rotor thrust-torque relationship is dependent upon the absolute wind velocity and the wind heading under consideration.

## INTERACTION OF THE TAIL ROTOR INFLOW AND WAKE WITH MAIN ROTOR INFLOW AND WAKE AS THE WIND HEADING AND VELOCITY ARE CHANGED

In this section, the same mental visualization procedures will be employed as in the previous section. However, the mental visualization of the basic flow patterns now requires consideration of both the overhead and the side viewing positions since the flow patterns now under consideration are more complex than the flow situation discussed in the preceding section.

Considering both the tail rotor and the main rotor wake without wind and out of ground effect, decompose the velocity vectors associated with the individual fluid elements comprising each wake into their axial and rotational components. The tail rotor wake intersects or joins with the main rotor wake at right angles, and in this interference region, the rotational component of the main rotor wake is in the opposite direction relative to the axial component of the tail rotor wake. The rotational component of the tail rotor wake (in the interference region) is in the same direction as the axial component of the main rotor wake. Because of the combination of the velocity vectors of the two wakes, the tail rotor is deflected slightly downward and, at the same time, curls around the outer periphery of the main rotor wake.

Reviewing the flow pattern situation with the introduction of wind at a heading of 90 degrees, and continuing the situation of out of ground effect, the combination of the inflow and wake trajectories of fluid elements associated with the main rotor disc region produces a pre-rotation or swirl of the inflow streampaths into the tail rotor. For a pusher tail rotor configuration, this induced pre-rotation of the inflow to the tail rotor coincides with the rotational direction of the tail rotor. As a consequence, it would appear reasonable that, with the main rotor

20

operating, the required tail rotor pitch setting would be somewhat greater than it would be without the main rotor operating.

Considering the situation with the wind at a heading of 270 degrees, the action of the main rotor inflow and wake with reference to inducing pre-rotation to th  inflow to the tail rotor is not quite as pronounced as for the 90-degree wind heading because of the required 180-degree turning of the flow as it enters the tail rotor disc. However, for this situation, the rotational component of the main rotor wake enhances the wind velocity vector and in doing so augments the tendency for the tail rotor wake to be blown back and reingested.

It will be recalled that with wind headings of 0 or 180 degrees, the inflow and wake patterns of an isolated rotor duplicated each other. With the main rotor operating, the situation changes significantly. With the wind at a 0-degree heading, the inflow to the tail rotor is under the direct influence of the main rotor wake, which, at the higher wind velocities, is transported back and into the tail rotor, particularly in the region associated with the lower half of the tail rotor disc. This flow situation also introduces pre-rotation of the flow into the tail rotor disc, but the major significance appears to be related to the difference in the inflow to the lower half of the tail rotor disc area which is under the influence of the main wake, compared with the inflow to the upper half of the tail rotor disc which is not.

With the wind at a 180-degree heading, the main rotor wake is blown away or downstream from the tail rotor; thus its influence on tail rotor performance at the higher wind velocities is negligible. At velocities, above the order of 15 knots, the tail rotor inflow approaches conditions similar to that of an isolated tail rotor.

The flow situations just reviewed were those wherein a ground plane was not present. With the insertion of a ground plane, significant changes occur in the inflow and wake pattern of both the main and tail rotors. The major cause of these changes is the main rotor wake, which upon impingement with the ground plane spreads outward and then rolls up in a process reminiscent of a standing vortex. For the hover condition, the standing vortex can be characterized as a ring vortex. With the introduction of wind, this standing ring vortex degenerates into a horseshoe-shaped vortex with the open end of the horseshoe downstream. At wind velocities of the order of 20-25 knots, the angle of impingement of the main rotor wake with

21

the ground plane is such that no roll-up of the wake occurs on the upstream side, i.e., the closed end of the horseshoe, although there is some impingement and roll-up of the wake along the ground plane parallel with the direction of the wind, i.e., the open end of the horseshoe. At wind velocities above the order of 25-35 knots, the main rotor wake no longer impinges on the ground plane in the region beneath the main rotor. The absolute wind velocity at which this impingement ceases is dependent on the main rotor lift value.

Turning now to a review of the tail rotor region flow conditions with wind, consider first the situation with the wind at a heading of 90 degrees. The influence of the main rotor wake and its formation into a rolled-up vortex on the ground plane is of concern at wind velocities from about 10-25 knots. Above 25 knots, the impingement of the main rotor wake against the ground plane occurs downstream of the tail rotor location, and therefore it no longer influences the flow patterns associated with the tail rotor inflow. However, the inflow of the main rotor influences the inflow to the tail rotor over the entire wind velocity range examined. As mentioned before, the nature of the inflow to the main rotor is such as to produce a pre-rotation of the flow entering the tail rotor disc area. In addition, the wind has the effect of "stretching" the tail rotor (downstream) before it mixes with the main rotor wake and inflow.

At a 270-degree wind heading, the reflection of the main rotor wake from the ground plane again influences both the inflow and wake pattern to the tail rotor for velocities from about 10-25 knots. As with the wind at a 90-degree heading, above 25 knots, the impingement of the main rotor wake with the ground plane also occurs downstream such that it no longer has an influence on the inflow to the tail rotor. The wind at this heading has a particularly strong influence on the wake of the tail rotor in that, as the velocity increases, the wind causes the tail rotor wake to blow back upon itself and in this manner becomes reingested. In blowing back, some of the tail rotor wake is also ingested by the main rotor.

Test conditions with the wind at a 180-degree heading, and covering a sector of the order of 45 degrees to either side of the 180-degree azimuth, afford the most interesting observations of main rotor wake impingement with the ground plane and its resulting influence on the tail rotor inflow and wake patterns. As mentioned earlier, the main rotor wake impinges against the ground plane and spreads radially outward, ultimately rolling up into a standing vortex, which at hover is a ring vortex. With the wind at the 180-degree heading, the position of this rolled-up or standing vortex

22

is shifted from a position upstream and away from the inflow region of the tail rotor to locations closer and closer to the tail rotor as the wind increases. At wind velocities of the order of 10 knots, the position of the standing vortex on the ground plane is just upstream of the tail rotor. At winds of the order of 12-13 knots, the position of this standing vortex is such that it appears to produce the maximum influence on both the inflow and wake characteristics of the tail rotor. At a velocity of the order of 15 knots, the rolled-up vortex is formed downstream of the tail rotor location, and thus its influence declines.

The critical situations can therefore be characterized as existing for wind velocities of the order of 10-15 knots and wind headings of the order of 120-250 degrees. Over this sector of wind headings, the presence of the rolled-up vortex on the ground plane can and does significantly influence the tail rotor inflow and wake by forming in the immediate vicinity of the tail rotor. At a wind heading of 180 degrees, it appears that the maximum influence should occur for winds of the order of 12-13 knots, while a wind heading of 225 degrees probably produces maximum influence at a wind velocity closer to 15 knots. The powerful influence of the standing vortex formed on the ground plane appears to be associated with the combination of its rotational velocity vectors in conjunction with the axial velocity vectors of the main rotor wake and the rotational direction of the tail rotor. Because of the manner in which these individual velocity vectors unite, the resultant velocity vector approaching the tail rotor blades is drastically altered as the standing vortex passes from a location directly upstream to one directly downstream of the tail rotor inflow region.

With the wind at a 0-degree heading, the inflow and wake patterns of the tail rotor with a ground plane are very similar to those without a ground plane. For example, at a zero wind velocity, the standing vortex created by impingement of the main rotor wake with the ground plane occurs well downstream and outside of the range wherein it can influence the inflow or the wake of the tail rotor. Thus this situation with a ground plane is similar to that without a ground plane. As the velocity increases, that portion of the standing vortex originally nearest the tail rotor location is projected further downstream and rapidly ceases to exist as that portion of the standing vortex becomes the open end of the horseshoe shape. The closed portion of the horseshoe shape formed by the standing vortex never approaches the tail rotor disc area since impingement and roll-up of the wake with the ground plane no longer occur when the velocities exceed the order of 20-25 knots, and wind

23

velocities higher than this are required to deflect the main
rotor wake so that impingement occurs in the tail rotor
region.

## EFFECT OF THE TAIL BOOM AND TAIL FIN ON TAIL ROTOR INFLOW AND WAKE, AND POSSIBLE CHANGES IN TAIL BOOM DRAG AS THE WIND HEADING AND VELOCITY ARE CHANGED

In turning our attention to the influence of the tail boom
and tail fin on directional control, the effect of the wind
on the tail boom and its effect on the tail fin will be
examined separately.  With the exception of winds centered
about and in the general region of headings of 180 degrees,
the tail boom is always submerged in the main rotor wake, at
least to wind velocities of the order of 25 knots.  The
rotational component of the main rotor wake always impinges
on the port side of the boom; thus this rotational component
of the main rotor wake coupled with the corresponding low
pressure on the downstream side of the tail boom always
produces a force which augments the tail rotor thrust in
maintaining directional control.  Wind headings of 0 and 180
degrees introduce no force on the boom.  The maximum
influence of the wind on the boom occurs at a heading of 270
degrees, where it augments the tail rotor thrust, and again
at a heading of 90 degrees, where it subtracts from the tail
rotor thrust.

The flow about the tail fin is believed to be primarily
controlled by the action of the tail rotor itself; thus the
influence of the wind on the tail fin (by itself) is believed
to be negligible in terms of affecting directional control.
The presence or lack of a ground plane is not believed to
have any effect on the influence of the wind on the tail boom
or tail fin.

## ANALYSIS OF THE TAIL ROTOR INFLOW AND WAKE PATTERNS IN CONJUNCTION WITH TAIL ROTOR PITCH SETTINGS FOR PUSHER AND TRACTOR CONFIGURATIONS

If the flow patterns discussed in the preceding sections are
now considered in conjunction with the tail rotor pitch
settings required during operation of the full-scale vehicle,
this additional information may be used to help clarify and
interpret the effects of the different variables affecting
the flow patterns about the helicopter (model) and thereby
also aid in understanding the variations in required tail
rotor thrust.

Tables III and IV presented the tail rotor pitch settings

24

required for both the tractor and pusher configurations of the helicopter studied in model scale during this investigation.  This information, obtained from flight data and through USAAVLABS, permits a recognition of some of the difficulties encountered when working with full-scale data. The first inconsistency noted in the tables is the tail rotor pitch setting(s) required for a zero wind velocity as a function of wind direction (heading).  It appears that different tail rotor settings are required solely as a function of wind direction.  Obviously, if no wind is present, vehicle orientation with reference to the wind is not a definable characteristic.  Therefore, the noted differences in the required tail rotor pitch settings with a zero wind velocity are either errors in determining the tail rotor pitch setting or the possibility that some wind did exist, or a combination of these factors.

However, while there is some question as to the accuracy of the tabulated information, it should be possible to deduce qualitative trends from these data which will augment the insight gained from the flow patterns observed during the experimental studies.  But before doing so, one other factor should be mentioned when this data is employed in interpreting the influence of the flow patterns on tail rotor thrust performance.  That factor is that the main rotor cyclic pitch control is tied in with the tail rotor pitch setting; thus it is impossible to separate the influence of either main rotor cyclic or tail rotor pitch as independent variables.

Consider first the matter of a pusher or tractor tail rotor configuration with a zero wind condition.  With no wind present, any difference in the required tail rotor pitch settings should be directly attributable to the tail rotor location relative to the tail fin.  Tables III and IV present no clear-cut evidence, but out of the 12 pitch settings listed for the zero wind condition, the pusher configuration lists five 11-degree situations while the tractor configuration always requires pitch settings greater than 11 degrees.  Therefore, it appears, on this basis, that the tractor tail rotor configuration requires slightly higher pitch settings than the pusher tail rotor configuration to maintain directional control when no wind is present.  This conclusion at least implies that for the condition of un-altered inflow to the tail rotor, i.e., the tractor configuration, less thrust is produced than for the case where the inflow to the tail rotor is subjected to passing about the tail rotor fin prior to entering the tail rotor, i.e., the pusher configuration.  However, the fact that the direction of rotation of the tail rotor is changed between tractor or pusher configuration cannot be completely ignored,

25

particularly when one recognizes how the components of the tail and main rotor inflow and wake interact with each other. However, this indication that the tractor tail rotor configuration seems slightly less effective than the pusher configuration is also augmented by examining all 60 conditions listed in Tables III and IV. Reviewing the information in the tables, it can be determined that the higher pitch setting is required by the tractor configuration in 34 of the cases listed. For 15 of the listed cases, the pusher configuration requires the higher tail rotor pitch setting, and for 11 cases there is no difference. It should be pointed out that no conclusion can be drawn from this information with regard to the tail rotor torque requirements since it is possible that a given tail rotor pitch setting may produce more thrust and consequently require more torque because of changes in the inflow or wake patterns.

The material in Tables III and IV does, however, permit additional substantiation of comments offered earlier. For example, considering the case of a 90-degree wind heading, the higher wind velocities indicate that greater tail rotor pitch settings are required in order to maintain directional control than are required for wind headings of the order of 270 degrees, for both the tractor and pusher configurations. This required difference in tail rotor pitch setting agrees with the earlier discussions of the flow patterns concerning an isolated tail rotor. There it was pointed out that the introduction of wind at a heading of 90 degrees was comparable to an axial $\Delta$-velocity increase in the inflow velocity vector to the tail rotor; thus higher tail rotor pitch settings would be required to produce the same thrust as that produced without the presence of the wind.

It might be of value to examine once more the data contained in Tables III and IV, this time with reference to the maximum tail rotor pitch setting required to maintain directional control. The choice between a pusher or a tractor tail rotor configuration may well be determined by the limiting operating conditions; on this basis, the tractor configuration seems to be the better choice. The pusher tail rotor arrangement requires the maximum geometric tail rotor pitch setting for operation over the wind heading sector of about 195-240 degrees and requires this maximum pitch setting when encountering the relatively low wind velocity of 10 knots. Also, the pusher tail rotor configuration requires the maximum pitch setting with a zero wind heading and a velocity of 30 knots. The tractor tail rotor configuration requires the maximum tail rotor pitch setting with the wind in the heading region of 90 degrees and for velocities above 15 knots. Thus, from an operational standpoint, the tractor

26

configuration seems preferable, since conditions requiring
the maximum tail rotor pitch setting by the pusher
arrangement are much more likely to occur than the
conditions requiring the maximum tail rotor setting for
tractor operation. In other words, operations with a wind
velocity of 10 knots and the wind at headings in the sector
of 195-240 degrees, or with zero heading and a velocity of
30 knots, are much more likely to occur than operations
with a wind heading around 90 degrees and wind velocities
above 15 knots.

## WAKE OBSERVATIONS, ANALYSIS, AND DISCUSSION

Directional control of a helicopter in the horizontal plane
is maintained during flight by balancing the two factors of
torque of the main rotor with thrust of the tail rotor.
Therefore, any analysis of directional control must, by
necessity, include data applicable to both factors. Of
course, the tail rotor must balance the torque of the main
rotor if directional control is to be achieved, but an
understanding of both factors is required if the most
effective control system is to be obtained.

Unfortunately, information which permits an examination of
the tail rotor pitch setting in conjunction with main rotor
cyclic and/or collective pitch settings was not available
through USAAVLABS. While that information would not be as
desirable in effective interpretation of the inflow and
wake observations as data obtained from a controlled study,
it would have permitted an additional approach or an
alternate method of separating the interaction and sub-
sequent effects of the main and tail rotor inflow and wake
in understanding helicopter directional control performance.

Four factors are of major importance in this test program:

1.  The importance of the presence or absence of
    a ground plane, particularly with winds up to
    25 knots and covering an azimuth sector of
    100 degrees centered about a wind heading of
    180 degrees.

2.  The interaction of the tail rotor wake with
    the inflow to the main rotor, the significance
    of main rotor inflow on tail rotor inflow, and
    the minimum influence of main rotor wake on
    tail rotor inflow and wake except when the
    main rotor wake impinges on the ground plane
    and is reflected into the tail rotor inflow
    area.

27

3. The minor effect that jet engine exhaust has on the wake patterns. (Note: the jet exhaust studies were performed out of ground effect only).

4. The annulus nature of the tail rotor wake which results because of the concentration of wake momentum near the outer periphery of the tail rotor wake, since all radial sections of the tail rotor are at the same pitch setting.

While the above factors are listed in order of their importance, development of a logical presentation of the knowledge gained during this study should perhaps start with the interaction of the main and tail rotor wakes rather than the inflow situations and then proceed from that situation.

When viewed from either the side or the overhead position, the tip vortex trails produced by an isolated main rotor in the hover mode form a concentric helix pattern. This pattern is shown in Figure 5. With the introduction of a uniform stream velocity (simulating wind), the tip vortex trails become skewed, but the basic symmetry of the wake pattern persists. This is shown in Figure 6, where the wake patterns associated with a simulated wind velocity of 35 knots are viewed from both the overhead and the side positions. (Arrows on the photographs show the general wind direction.)

When a complete helicopter model is tested, the interaction of the tail rotor wake with the main rotor inflow and wake is most evident. Figure 7 is an overhead view illustrating how the main rotor tip vortex wake trails are distorted by ingestion of the tail rotor wake by the main rotor. A side observation of tail rotor wake ingestion by the main rotor is shown in Figure 8. The importance of a distortion in the inflow streampaths and the resulting effect on rotor thrust and torque characteristics should not be minimized. The importance of inflow perturbations and their effect on airfoil performance are well known [10, 11]. Also, the influence of inflow velocity perturbations on thrust and torque characteristics has received considerable attention in the marine propulsor field [12, 13]. Therefore, it seems prudent to suggest that the degree of main rotor torque fluctuations resulting from tail rotor wake ingestion is a fruitful field of investigation if a complete understanding of the helicopter directional control problem is desired.

That the action of the main rotor drastically alters the inflow and wake patterns of the tail rotor should come as no surprise, but the degree of distortion is usually considered remarkable when viewed for the first time. Figures 9 through 13 illustrate how the tail rotor wake is altered through

28

operation of the main rotor. These observations are made from an overhead viewing position for specific wind headings and velocities, both with and without main rotor operation. The tail rotor wake was made visible by bleeding air from one tail rotor tip, and the photographs were taken at the relatively slow exposure time of 1/60 second to permit a streak photograph of the tip vortex trail(s) to be obtained, rather than a photograph wherein the individual tip vortex trails are stopped. All photographs in this series of five figures were taken at the hover condition and with equivalent wind velocities of 15 and 30 knots. There is no ground plane present in any of these figures.

Figure 9 presents views of the tail rotor wakes associated with a wind heading of zero degrees. Of particular interest are Figures 9(a) and 9(d), which show the effect of main rotor operation in hover. Figure 10 presents photographs with a wind heading of 180 degrees, while Figure 11 presents photographs with a wind heading of 230 degrees. Figures 11(c) and 11(f) are for a 30-knot wind condition and offer good observations of the nature of the blowback and re-ingestion of the tail rotor wake by the tail rotor due to the action of the wind both with and without main rotor operation. Figure 12 presents photographs for a wind heading of 250 degrees. In this figure, the 15-knot velocity case, Figure 12(e), offers a good observation of the manner in which the outer periphery of the tail rotor wake is expanded or mushroomed outward by the impingement action of the wind. This expansion of the tail rotor wake, which is believed to result from the fact that the majority of the wake momentum is concentrated in the outer periphery, has been mentioned in earlier discussions. Figure 13 presents photographs for a wind heading of 270 degrees. Figures 13(e) and 13(f) again offer good observations of the blowback and reingestion of the tail rotor wake by the tail rotor. Of course, as mentioned before, the main purpose of this series of figures is to show how the tail rotor wake is altered by operation of the main rotor. Because of the variation in this effect, individual examination of all photographs in the figures is required for a thorough understanding of this interaction.

Several side observations of the tail rotor wake when out of ground effect are shown in Figures 14 and 15. The photographs comprising these figures illustrate the manner which the tail rotor wake is drawn upward and then into the main rotor disc area by the action of the inflow into the main rotor. These figures, in conjunction with the immediately preceding series of photographs, illustrate the manner in which interaction of the tail rotor wake and main rotor inflow can occur.

The series of photographs shown in Figures 16 through 24 illustrates inflow patterns to the tail rotor, how this inflow is affected by main rotor operation in the presence of a ground plane, and how the tail rotor wake interacts with the main rotor inflow under these conditions.  As mentioned in earlier discussions, one of the observations of major importance associated with this study concerned the impingement of the main rotor wake with the ground plane, its roll-up into a standing vortex, and how this rolled-up vortex affected the inflow to the tail rotor.

In the absence of wind or hover operation of the main rotor, the streampath inflow to the tail rotor forms the classical "sink" pattern.  This pattern is shown in Figure 16.  The introduction of a 10-knot wind at a heading of 180 degrees produces inflow patterns as shown in Figure 17 when the model is viewed from the side.  The upper photograph in this figure shows the inflow pattern associated with the main rotor not operating while the lower photograph was taken with the main rotor operating.  Without main rotor operation at this 10-knot velocity, the classical inflow streampaths to the rotor still occur, but the relatively small disturbance of the lower dye streak clearly indicates the localized extent of tail rotor inflow on the region surrounding the tail rotor location.  With main rotor operation, the outer boundary of the main rotor wake roll-up is clearly defined by the presence of the dye.  The "eye" of the rolled-up vortex is clear of dye.  The portion of the vortex can be seen to be just upstream of the tail rotor. While this photograph may indicate that the flow into the tail rotor is rather badly confused, an overhead view for the same 10-knot condition presented in Figure 18 shows the degree of disturbance.  This figure shows the uniform inflow to the tail rotor without main rotor operation and the extent of flow disturbance existing in the tail rotor inflow region when the main rotor is operating.

Increasing the wind velocity to 15 knots and retaining the 180-degree heading produces the inflow patterns shown in Figure 19 for a side viewing position and in Figure 20 for an overhead viewing position.  From these figures it can be seen that the roll-up of the vortex formed by main rotor wake impingement on the ground plane no longer influences the inflow to the tail rotor or the tail rotor wake.  This is shown particularly well in the overhead viewing position photographs, where the dye streampaths into the tail rotor are clearly undisturbed.  The critical wind velocity at the 180-degree heading, in terms of positioning the main rotor rolled-up vortex in the region of the tail rotor so as to produce the maximum change in tail rotor thrust performance, occurs, as was mentioned in earlier discussions, between

30

12 and 13 knots.

Side viewing position observations indicating how the location of the main rotor wake and its impingement on the ground plane are altered as the wind heading is changed are shown in Figure 21. In this series of photographs, the wind velocity is 15 knots and the wind headings illustrated are for 180, 195, 210, and 225 degrees. From a viewing of these photographs, the inflow patterns might be interpreted as indicating that considerable disturbance exists in the inflow region to the tail rotor. Figure 22, comprised of overhead position photographs of the same conditions, shows that this is not true. The unconfused inflow patterns to the tail rotor with main rotor operation are clearly established, and Figure 23 shows that they do not vary significantly from the inflow patterns existing without main rotor operation.

The combination of main rotor and tail rotor interactions on each other's inflow and wake pattern is perhaps best characterized by viewing the situation with a wind heading of 90 degrees. In Figure 24, conditions with the main rotor operating and not operating are shown for wind velocities of 10, 15, and 25 knots. The left-hand series of photographs presents the inflow and wake patterns associated with the main rotor not operating. These photographs are of particular interest since they illustrate the earlier-mentioned observation that the presence of the wind at a heading of 90 degrees reduces the effective pitch setting of the tail rotor. All of the tests performed in the presence of the ground plane were taken with a single tail rotor pitch setting. Therefore, any change in the inflow or wake patterns cannot be related to changes in tail rotor pitch setting. In producing thrust, the streampaths passing through a rotor or propeller disc area are contracted. From the photograph associated with the 10-knot wind velocity case, Figure 24(a), it is clearly evident that the dye streaks, upon passing through the tail rotor disc area, are rather sharply contracted, thus indicating that thrust is being produced. With a wind velocity of 15 knots, Figure 24(b), the contraction of the dye streaks entering the tail rotor disc area is almost negligible; thus in actual practice, the geometric tail rotor pitch setting would have to be increased over that required at 10 knots to maintain the same amount of tail rotor thrust or the same degree of directional control. (That an increase in the tail rotor pitch setting is necessary with a change in the velocity from 10-15 knots with a wind heading of 90 degrees can be verified by referring to Tables II and III.) At a 25-knot wind condition, Figure 24(c), no contraction of the dye streams entering the tail rotor disc area is evident, indicating that the tail rotor pitch setting would have to be increased once again to produce thrust.

31

Turning our attention to the configuration with the main rotor operating, the situation for a 10-knot wind velocity, Figure 24(d), shows that the dye streaks approaching the tail rotor disc area are being retarded and prevented from entering the tail rotor disc area. This occurs as a result of the main rotor wake's impingement upon the ground plane and the main rotor wake's outward radial motion. At a wind velocity of 15 knots, Figure 24(e), some of the retardation of the inflow is still evident, but more important is the uplifting of the general inflow upstream of the model and its ingestion into the main rotor disc area. At a wind velocity of 25 knots, Figure 24(f), the lower dye streak clearly establishes the limit of the main rotor wake impingement and roll-up on the ground plane, while the upper dye streaks illustrate how the flow in the tail rotor region is influenced by main rotor inflow demands.

The path of the tail rotor wake as indicated by the air bubble streaks emitted from the tail rotor is also of considerable interest. Observe that in all of the photographs taken without main rotor operation, the tail rotor wake travels horizontal and parallel to the ground plane. With main rotor operation and at a wind velocity of 10 knots, the lower portion of the tail rotor wake interacts with the main rotor wake and thus is distorted in a downward direction toward the ground plane. At a wind velocity of 15 knots, some distortion of the tail rotor wake in the downward direction is still evident, but the influence of the main rotor wake appears to be decreased over the 10-knot case. However, at 25 knots, the wake of the tail rotor is projected in an upward direction. This occurs because the tail rotor wake is now influenced both by that portion of the main rotor wake traveling toward the ground plane and by that portion of the main rotor wake reflected upward after impingement with the ground plane. Under this 25-knot wind condition, the tail rotor wake is more closely aligned with the reflected portion of the wake than with the downward portion of the wake

## JET ENGINE EXHAUST

The studies involving an evaluation of the effect that jet engine exhaust had on the main-rotor/tail-rotor interaction were made for the out-of-ground-effect condition only. Observations with the pusher tail rotor configuration were made both with and without simulated jet engine exhaust. No significant change in either the tail rotor wake or the nature of the interaction of the tail rotor wake with the main rotor wake could be noted for any of the wind velocities or wind headings investigated. It did appear as if the interaction of the main rotor wake with the tail rotor wake

32

was slightly more pronounced when the jet engine exhaust was being simulated. This seems reasonable in that the velocity component of the jet engine exhaust would tend to distort the main rotor wake; thus the interaction at the interference plane of the tail rotor wake with the main rotor wake should be accentuated.

While no significant change could be noted in the tail-rotor interaction, in being completely objective it must be recognized that in actual operation, in addition to the jet velocity flow stream which was scaled in the model studies, the local air density changes during full-scale operation because of the higher temperature of the jet engine exhaust. This local change in air density could well influence the local thrust (and consequently torque) performance of both the main and tail rotors. Whether this occurs and the magnitude of this influence (if there is any) could not be ascertained in this study. What this study shows is that the velocity components of the jet engine exhaust do not influence the tail-rotor/main-rotor interaction patterns to any significant degree.

When studying the tractor tail rotor configurations, a series of photographs was taken at different equivalent jet engine exhaust velocities for different wind velocities at a wind heading of 180 degrees. This series of photographs is shown in Figures 25 and 26. Figure 25 presents photographs for the zero wind (hover) condition. The series (a) photographs present the flow patterns associated with jet engine exhaust without the main or tail rotor in operation. These photographs show that at a simulated jet exhaust velocity of 112 feet per second, which is well below the operational exhaust velocity of 226 feet per second, the jet engine exhaust has extended into the tail rotor region. At higher jet velocities, the exhaust projects well beyond the tail rotor region. The series (b) photographs present the same jet engine exhaust velocity conditions but with the main and tail rotors of the model now operating. From these photographs, it can be seen that the downwash from the main rotor deflects the simulated exhaust downward and that this downward deflection of the jet engine exhaust continues to equivalent jet engine exhaust velocities of 290 feet per second, or well above the operational jet exhaust velocity of 226 feet per second. At the equivalent full-scale operating condition of an engine exhaust velocity of 226 feet per second, the outer projection edge of the exhaust stream approaches the tail rotor region and, while it does not enter the tail rotor area, the influence of the main and tail rotor's wakes on the flow in the general area is evident.

33

In Figure 26, the flow conditions for equivalent wind velocities of 10, 20, and 30 knots at a heading of 180 degrees are shown. The only interaction of the jet engine exhaust with tail rotor flow at the operational jet exhaust velocity of 226 feet per second occurs with a 20-knot wind, and the interaction is with the wake, not the inflow side of the tail rotor.

## CONCLUSIONS

In this study, the interactions of the main-rotor/tail-rotor
wakes and inflow were examined. This information is of
value as input to the directional control problem which
exists with certain helicopter designs. The direct
observation of the inflows and wakes of both the main and
tail rotors has permitted a significant advancement in the
knowledge applicable to such flow situations. The major
conclusions of this investigation are:

1. The presence of a ground plane is important.
   With a ground plane, the main rotor wake of
   a helicopter (at hover) impinges against the
   ground plane and then spreads radially out-
   ward. At the outer periphery of this radial
   expansion, the wake rolls up into a standing
   vortex.

2. The introduction of a wind velocity component
   causes the location of the rolled-up vortex
   to shift on the ground plane and also changes
   the rolled-up vortex from one resembling a
   ring vortex to one which has a horseshoe shape,
   with the open end of the horseshoe downstream.
   The impingement and roll-up of the main rotor
   wake on the ground plane occurs to velocities
   of the order of 20 knots. Above that velocity,
   the wake from the main rotor does not impinge
   on the ground plane in the area directly
   beneath the rotor such that roll-up occurs.

3. With the introduction of winds covering an
   azimuth sector of the order of 100 degrees and
   with this azimuth sector centered above a heading
   of 180 degrees, it can be understood from 2, above,
   that the closed portion of the horseshoe-shaped
   rolled-up vortex will be positioned nearer and
   nearer the tail rotor as the wind velocity is
   increased. At some value of wind velocity,
   and depending upon the wind heading, the rolled-
   up vortex will be situated such that it has a
   maximum influence on the flow in and about the
   tail rotor region. For example, with a wind
   heading of 180 degrees, it appears as if the
   maximum influence on the tail rotor thrust should
   occur with wind velocities of the order of 12-13
   knots.

4. Ingestion of the main rotor wake by the tail rotor
   and the tail rotor wake by the main rotor both

occur under certain wind headings and wind velocities. From these flow observations, it appears as if ingestion of the tail rotor wake by the main rotor would have more influence on helicopter directional control then the reverse case of main rotor wake influence on the tail rotor, except for cases with a ground plane where the main rotor wake impinges, rolls up, and then becomes located in the tail rotor region. The influence of the tail rotor wake on main rotor ingestion and its subsequent influence on directional control, by affecting the torque of the main rotor, is associated with the recognized variation in the thrust and torque performance of lifting surfaces when subjected to inflow perturbations.

5. The annulus nature of the tail rotor wake, that is, the concentration of momentum in the outer periphery of the wake, appears to be a strong contributory factor to the unsteadiness of the tail rotor thrust, particularly when the wind impinges against the tail rotor wake.

6. The jet engine exhaust velocity component, at the operational exhaust velocity, appears to have little influence on the inflow or wake interaction patterns. However, it must be noted that these exhaust studies were taken for the situation of out of ground effect only and that local density differences in the test medium such as occurs under full-scale operation in air were not scaled.

7. Excluding wind headings of the order of 195-240 degrees at wind velocities of 10-15 knots, the inflow and wake of the tractor tail rotor configuration appear to have slightly more interaction with the main rotor wake and inflow than the pusher tail rotor configuration does. Examination of operational data confirms that slightly higher tail rotor pitch settings are required. However, at the wind headings of the order of 195-240 degrees and at wind velocities of 10-15 knots, the pusher tail rotor config- uration introduces the more significantly obvious tail-rotor/main-rotor wake and inflow mentioned; the pusher tail rotor configuration possesses the most unsteady tail rotor wake, i.e., the wake seems to pulsate when it is observed

with high-speed photography.  Therefore, on the
basis of flow observations alone, the tractor
tail rotor configuration seems to be a slightly
better choice than the pusher tail rotor
configuration.

# LITERATURE CITED

1. Payne, P. R., HELICOPTER DYNAMICS AND AERODYNAMICS, Sir Isaac Pitman & Sons, Ltd., London, 1959, p. 442.

2. Lehman, A. F., MODEL STUDIES OF HELICOPTER ROTOR FLOW PATTERNS, USAAVLABS Technical Report 68-17, U. S. Army Aviation Materiel Laboratories, Fort Eustis, Virginia, April 1968, AD671670.

3. Heyson, H. H., WIND-TUNNEL WALL EFFECTS AT EXTREME FORCE COEFFICIENTS, Presented at the International Congress of Subsonic Aeronautics (New York Academy of Sciences), New York, New York, April 3-6, 1967. (Available from NASA as TM X-59742.)

4. Heyson, H. H., SOME CONSIDERATIONS IN WIND-TUNNEL TESTS OF V/STOL MODELS, Presented at the University of Tennessee Space Institute, Tullohoma, Tennessee, Sept. 29, 1967. (Available from NASA as TM X-60772.)

5. Heyson, H. H., THE FLOW THROUGHOUT A WIND TUNNEL CONTAINING A ROTOR WITH A SHARPLY DEFLECTED WAKE, Presented in the Proceeding Third CAL/AVLABS Symposium, Volume II, Buffalo, New York, June 18-20, 1969.

6. Rae, W. H., Jr., LIMITS ON MINIMUM-SPEED V/STOL WIND TUNNEL TESTS, AIAA Journal of Aircraft, Volume 3, No. 4, 1967, pp. 249-254.

7. Rae, W. H., Jr., and Shindo, S., COMMENTS ON V/STOL WIND-TUNNEL DATA AT LOW FORWARD SPEEDS, Presented in the Proceedings Third CAL/AVLABS Symposium, Volume II, Buffalo, New York, June 18-20, 1969.

8. Lehman, A. F., and Besold, J. A., TEST SECTION SIZE INFLUENCE ON MODEL HELICOPTER ROTOR PERFORMANCE, USAAVLABS Technical Report 71-6, U. S. Army Air Mobility Research and Development Laboratory, Fort Eustis, Virginia (to be published).

9. South, P., RESEARCH ON REDUCTION OF WALL EFFECTS IN LOW SPEED WIND TUNNELS, DME/NAE Quarterly Bulletin, No. 1, April 1968, pp. 57-77.

10. Horlock, J. H., FLUCTUATING LIFT FORCES ON AEROFOILS MOVING THROUGH TRANSVERSE AND CHORDWISE GUSTS, Transactions of the ASME, Vol. 90, Series D, No. 4 December 1968, pp. 494-500.

11.    Dress, J. M., and Harvey, K. W., HELICOPTER GUST RESPONSE
       AT HIGH FORWARD SPEED, Journal of Aircraft, Vol. 7, No.
       3, May-June 1970, pp. 225-230.

12.    Tsakonas, S., Breslin, J., and Miller, M., CORRELATION
       AND APPLICATION OF AN UNSTEADY FLOW THEORY FOR PROPELLER
       FORCES, Transactions of the SNAME, Vol. 75, 1967, pp.
       158-193.

13.    Miller, M. L., EXPERIMENTAL DETERMINATION OF UNSTEADY
       PROPELLER FORCES, 7th Symposium on Naval Hydrodynamics,
       Rome, August 25-30, 1968.
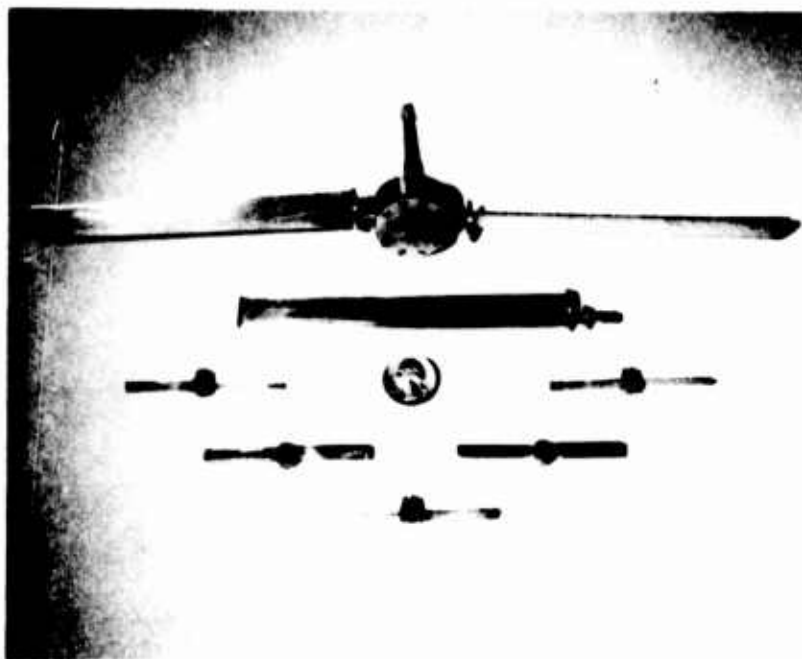
Figure 1. Main and Tail Rotor.
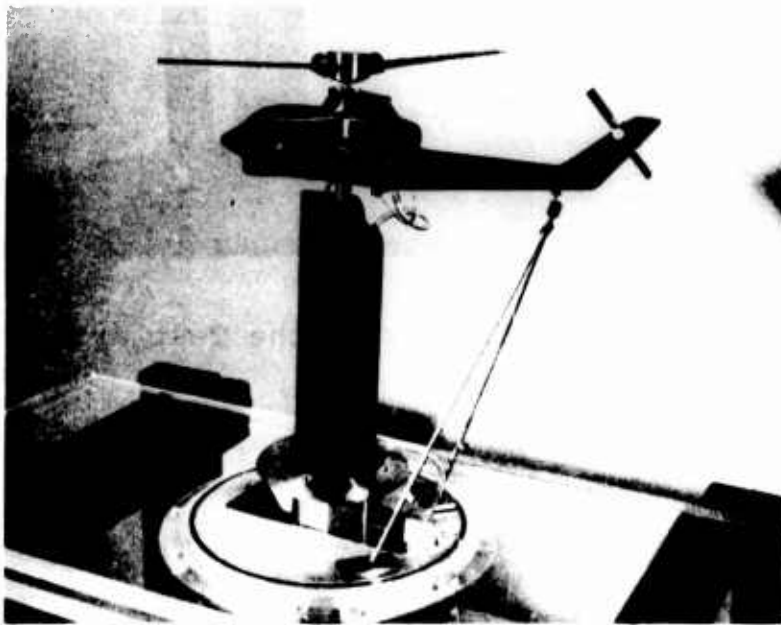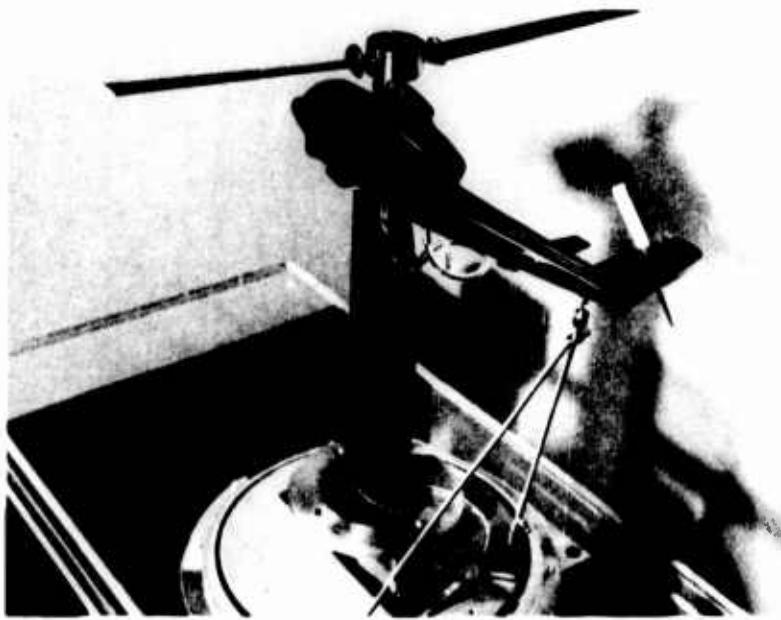
Figure 2. Two Views of the Model.
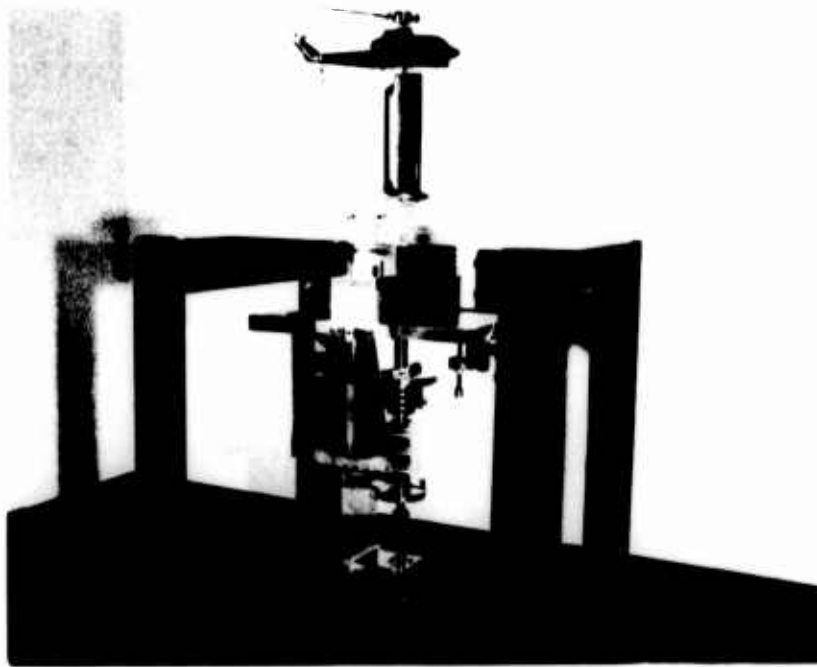
Figure 3. Overall View of the Test Arrangement.
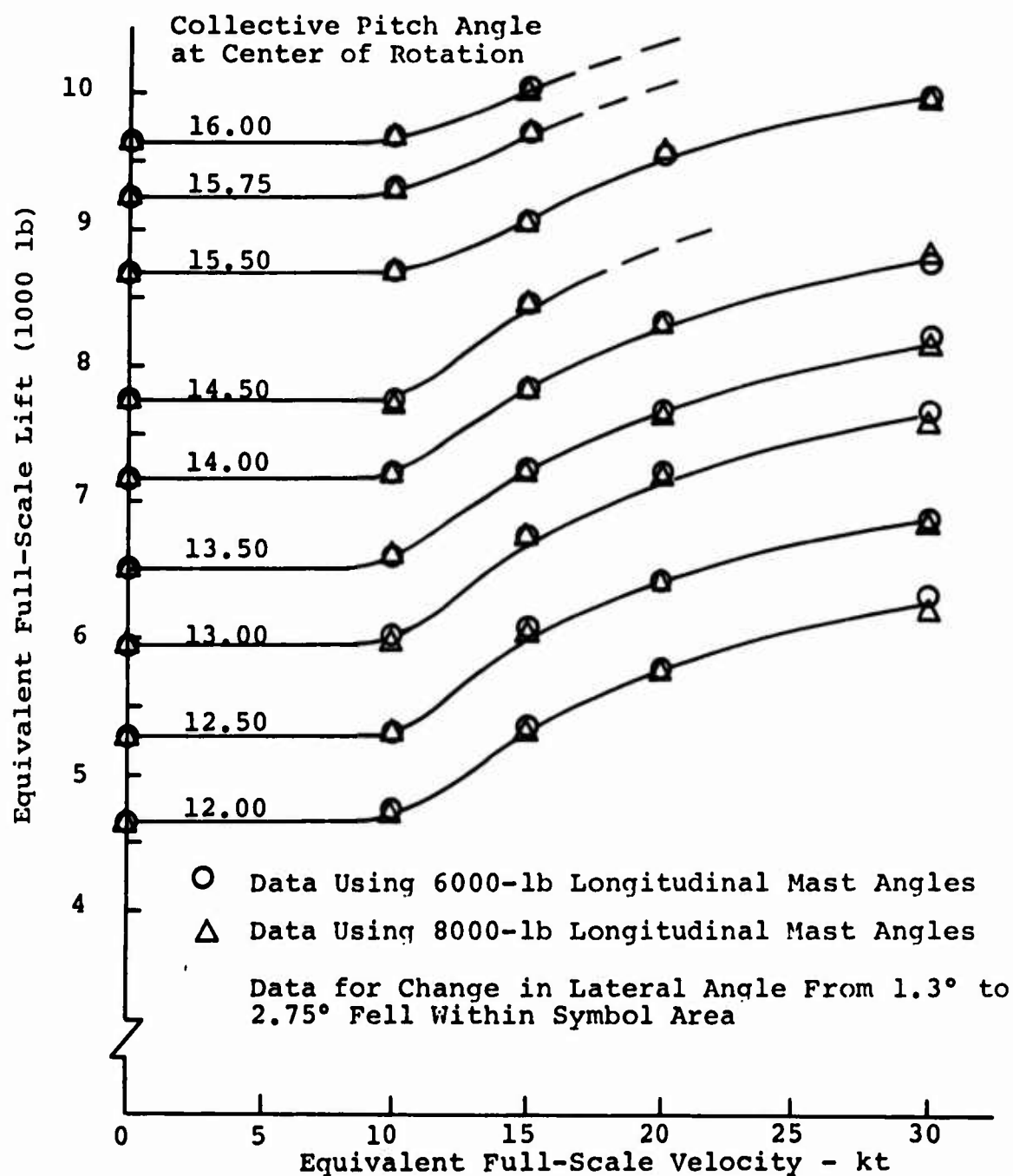
Figure 4. Equivalent Full-Scale Lift as a Function of Main Rotor Collective Pitch Angle and Forward Velocity as Determined From Model Tests.

43
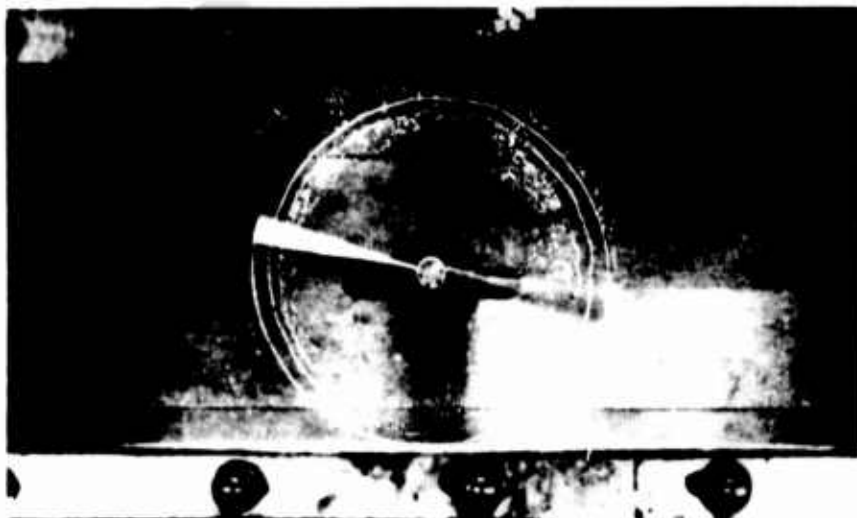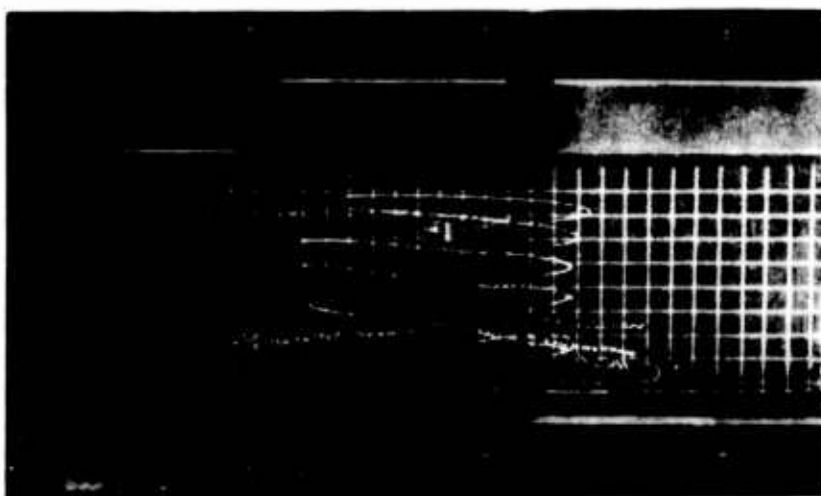
Overhead View



Side View

Figure 5.  Isolated Rotor at Hover Illustrating Tip
Vortex Trails.

44
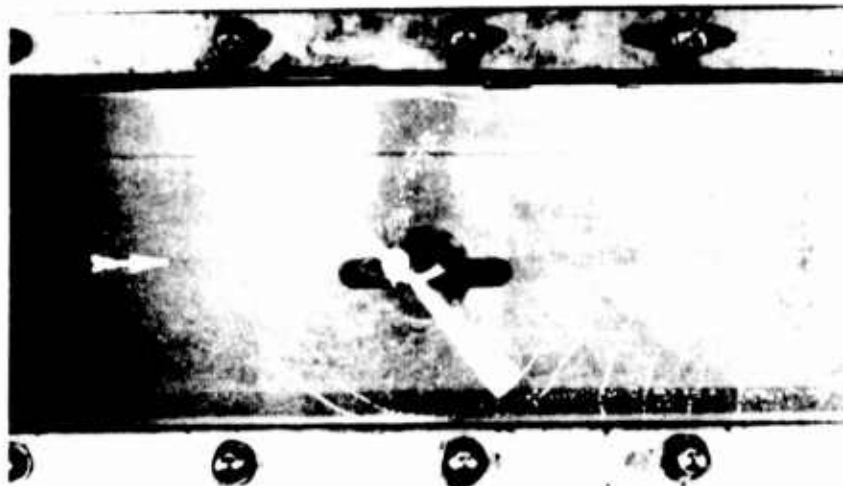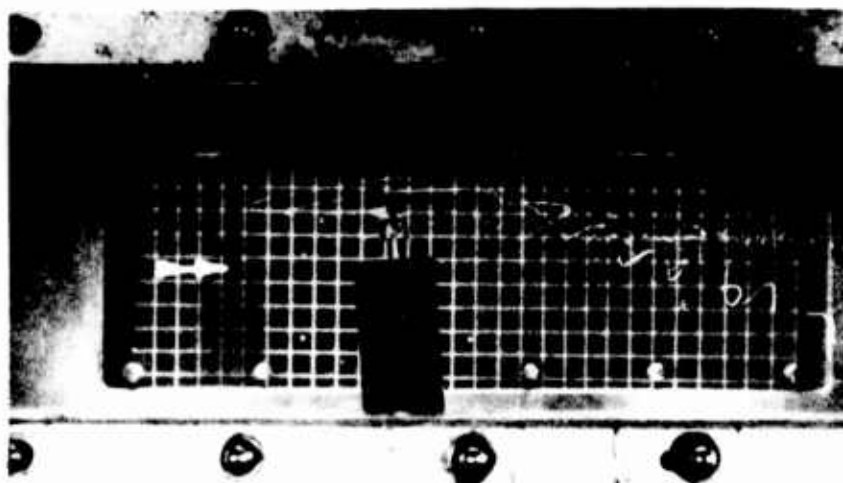
Overhead View



Side View

Figure 6.  Isolated Rotor Illustrating Tip Vortex Trails
at an Equivalent Wind Velocity of 35 Knots.

45
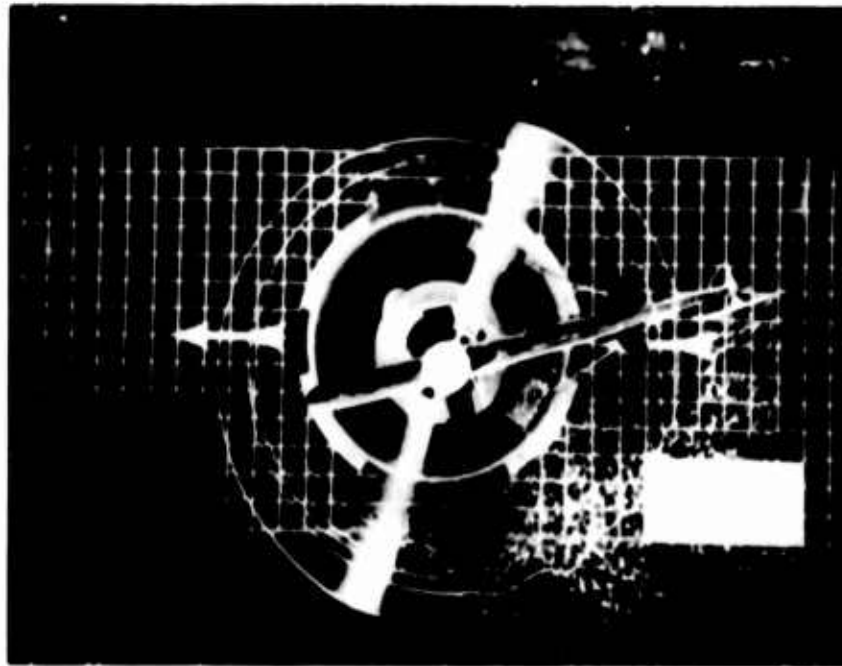
**Hover**
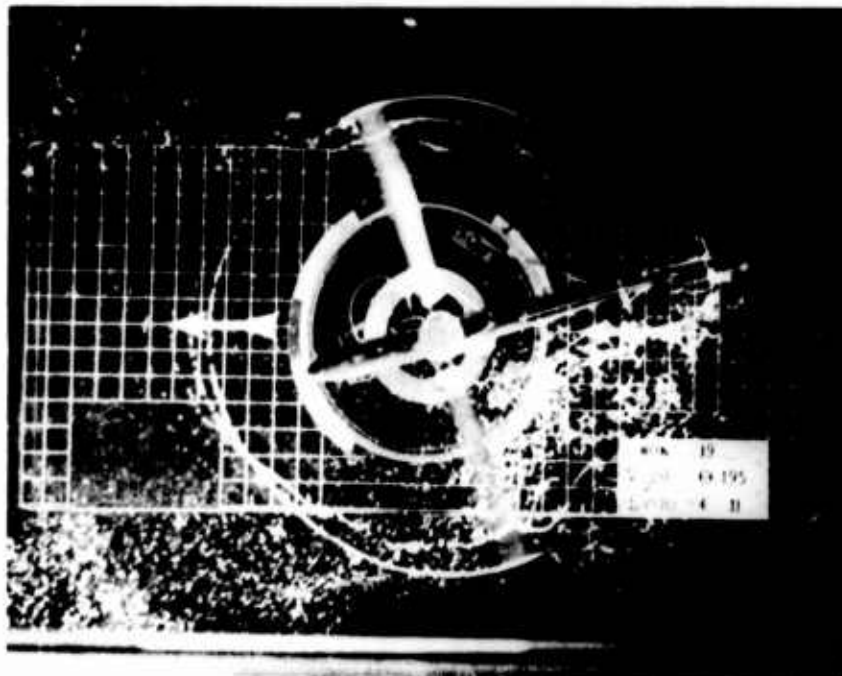


Velocity = 20 Knots with a Wind Heading of 195 Degrees

Figure 7.   Overhead Observations of the Distortion of the
Main Rotor Wake Through Tail Rotor Wake
Ingestion, Out of Ground Effect.

46

Figure 8.   Side Observation of the Distortion of the
            Main Rotor Wake Through Tail Rotor Wake
            Ingestion, Out of Ground Effect, in Hover.

(a)   Velocity 0 Kt
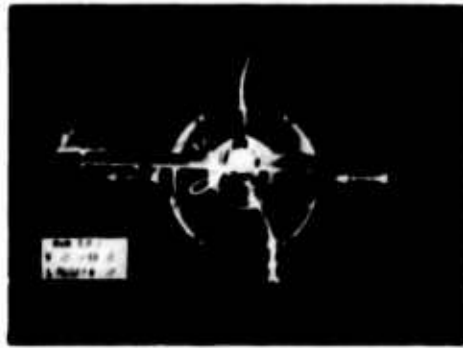
(d)   Velocity 0 Kt
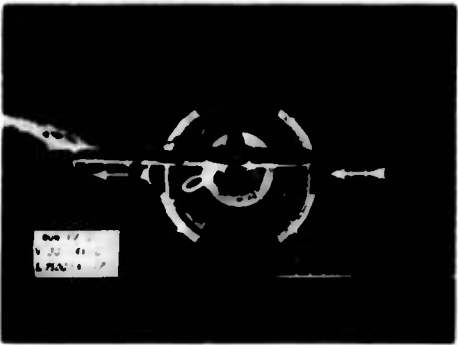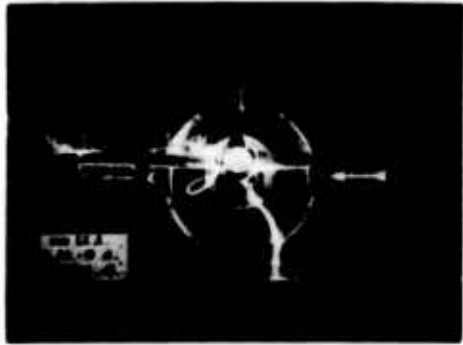
(b)   Velocity 15 Kt

(e)   Velocity 15 Kt

(c)   Velocity 30 Kt

(f)   Velocity 30 Kt

Series a, b, and c Without
Main Rotor

Series d, e, and f With
Main Rotor Operating

Figure 9.   Views of the Tail Rotor Wake at a 0-Degree
Wind Heading, Wind Velocities of 0, 15, and 30
Knots, With and Without the Main Rotor Operating.

48
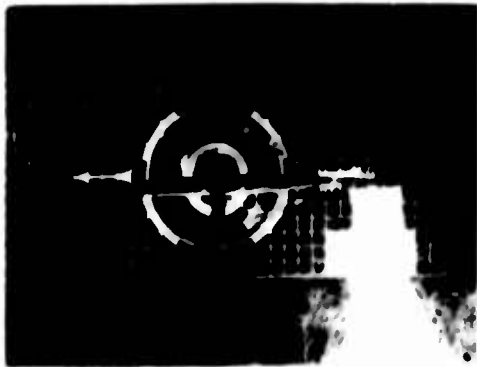
(a)   Velocity 0 Kt                    (d)   Velocity 0 Kt

(b)   Velocity 15 Kt                   (e)   Velocity 15 Kt

(c)   Velocity 30 Kt                   (f)   Velocity 30 Kt

Series a, b, and c Without         Series d, e, and f With
      Main Rotor                        Main Rotor Operating

Figure 10.   Views of the Tail Rotor Wake at a 180-Degree
             Wind Heading, Wind Velocities of 0, 15, and 30
             Knots, With and Without the Main Rotor Operating.

(a)   Velocity 0 Kt                (d)   Velocity 0 Kt
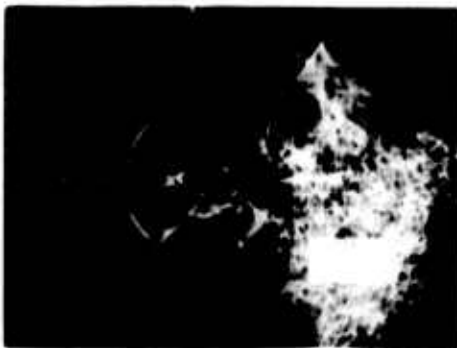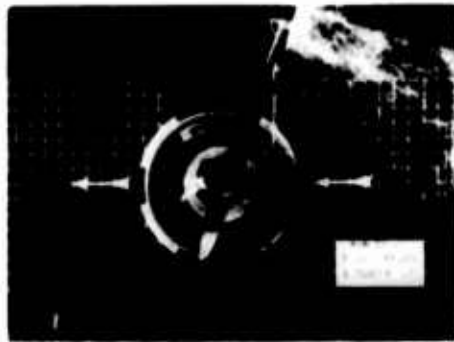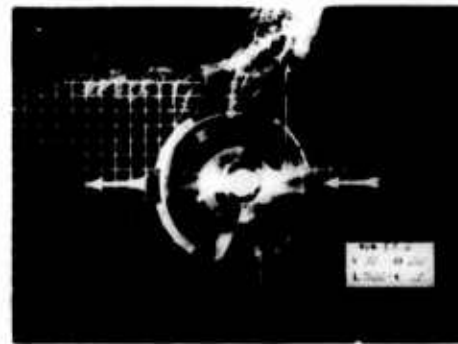
(b)   Velocity 15 Kt             (e)   Velocity 15 Kt

(c)   Velocity 30 Kt             (f)   Velocity 30 Kt

Series a, b, and c Without       Series d, e, and f With
Main Rotor                      Main Rotor Operating

Figure 11.   Views of the Tail Rotor Wake at a 230-Degree
Wind Heading, Wind Velocities of 0, 15, and 30
Knots, With and Without the Main Rotor Operating.

50

(a)   Velocity 0 Kt

(d)   Velocity 0 Kt

(b)   Velocity 15 Kt

(e)   Velocity 15 Kt

(c)   Velocity 30 Kt

(f)   Velocity 30 Kt

Series a, b, and c Without
Main Rotor

Series d, e, and f With
Main Rotor Operating

Figure 12.   Views of the Tail Rotor Wake at a 250-Degree
Wind Heading, Wind Velocities of 0, 15, and 30
Knots, With and Without the Main Rotor Operating.

51

(a)    Velocity 0 Kt
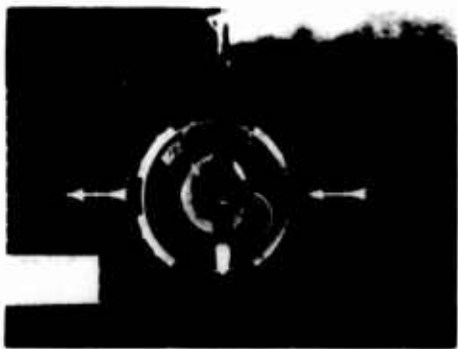
(b)    Velocity 15 Kt

(c)    Velocity 30 Kt

(d)    Velocity 0 Kt

(e)    Velocity 15 Kt

(f)    Velocity 30 Kt

Series a, b, and c Without          Series d, e, and f With
        Main Rotor                      Main Rotor Operating

Figure 13.    Views of the Tail Rotor Wake at a 270-Degree
              Wind Heading, Wind Velocities of 0, 15, and 30
              Knots, With and Without the Main Rotor Operating.
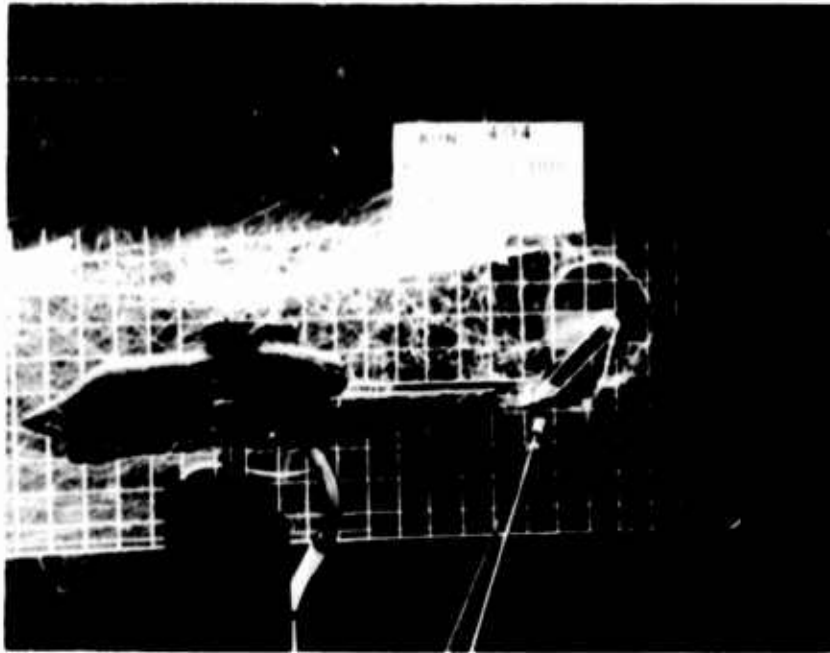
Wind Heading of 180 Degrees
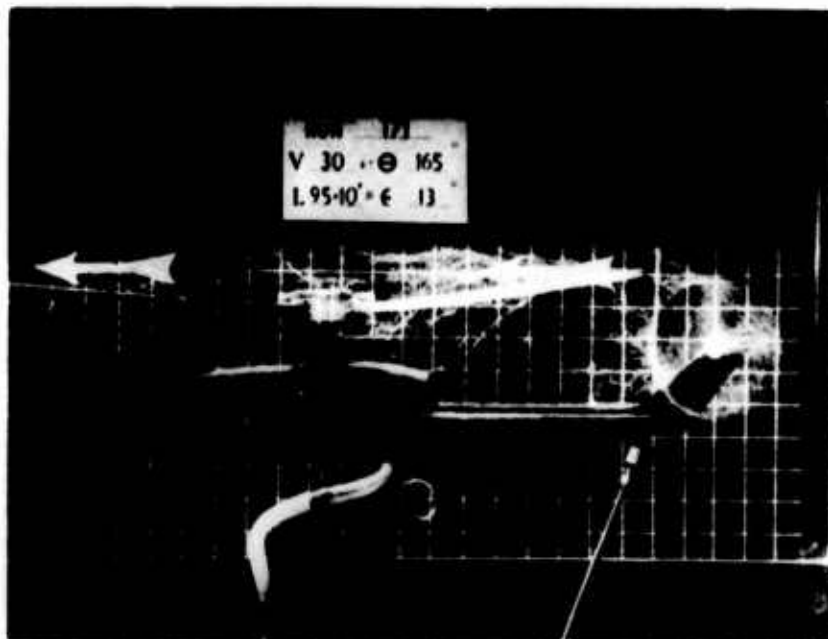


Wind Heading of 165 Degrees

Figure 14.  Side Observations of the Tail Rotor Wake
            Ingestion by the Main Rotor at an
            Equivalent Wind Velocity of 30 Knots.

53
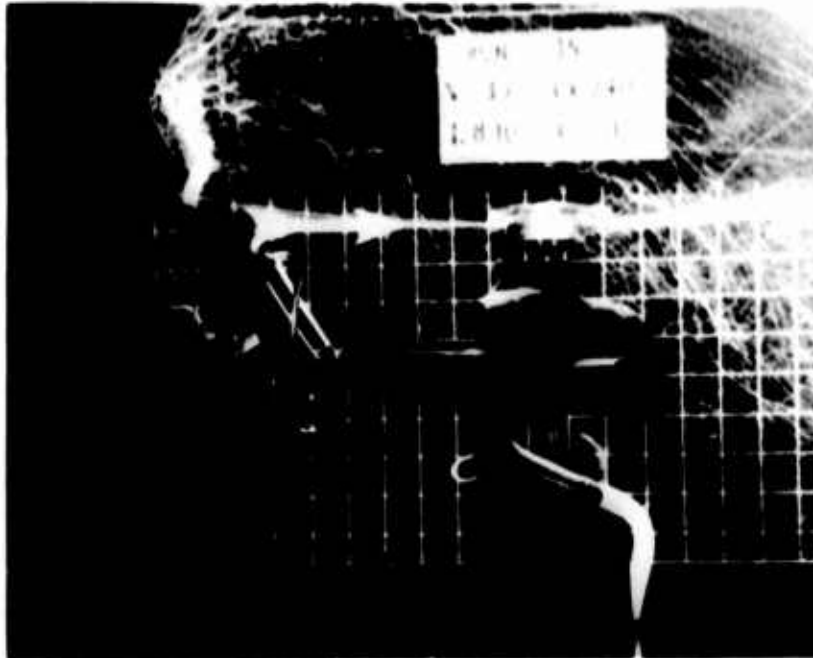
Note the lifting up and blowing back of the tail rotor
wake at this wind heading.

Figure 15.  Side Observation of the Tail Rotor Wake
            Ingestion by the Main Rotor at an
            Equivalent Wind Velocity of 30 Knots
            and a Wind Heading of 240 Degrees.

Figure 16.  Side Observation of Streampath Inflow Pattern
to the Tail Rotor Without the Main Rotor and
With No Wind.
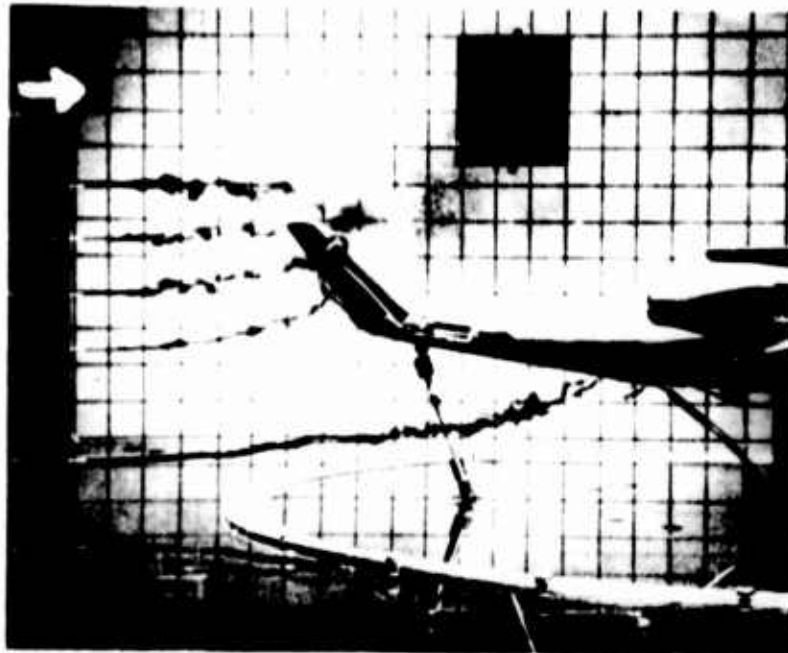
Without Main Rotor



With Main Rotor Operating

Figure 17. Side Observations of Streampath Inflow Pattern to the Tail Rotor With and Without Main Rotor. Wind Velocity of 10 Knots at a Heading of 180 Degrees.

56
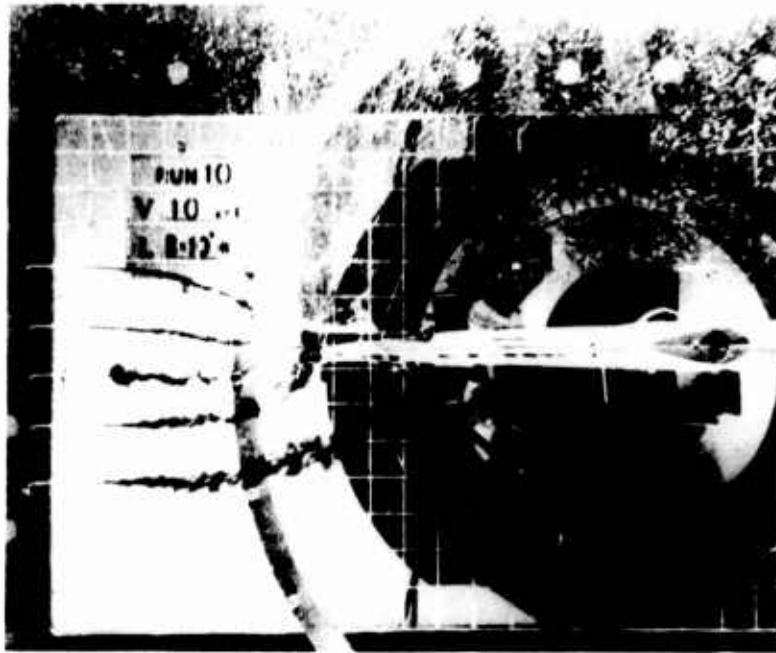
Without Main Rotor



With Main Rotor Operating

Figure 18.   Overhead Observations of Streampath Inflow Pattern
             to the Tail Rotor With and Without Main Rotor.
             Wind Velocity of 10 Knots at a Heading of
             180 Degrees.

57
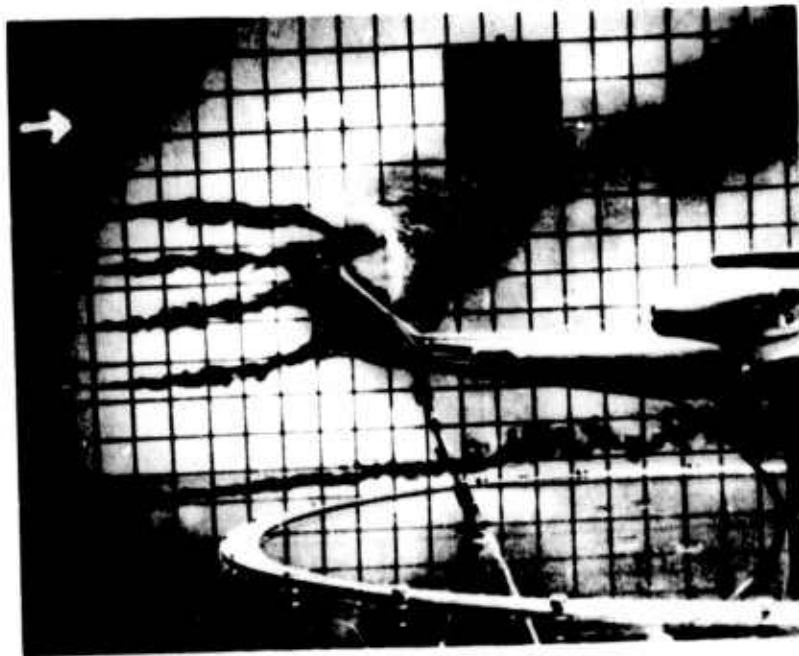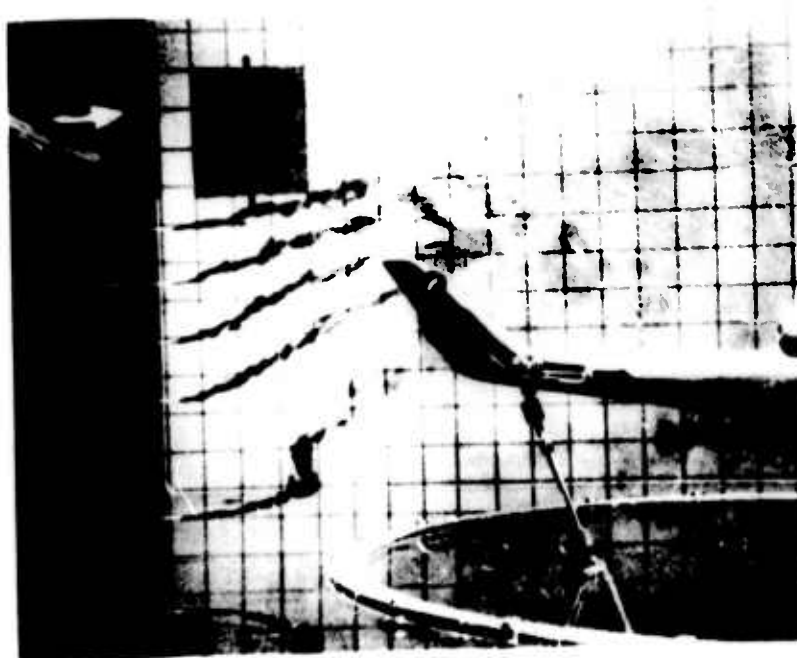
Without Main Rotor



With Main Rotor Operating

Figure 19.  Side Observations of Streampath Inflow Pattern
to the Tail Rotor With and Without Main Rotor.
Wind Velocity of 15 Knots at a Heading of
180 Degrees.

58
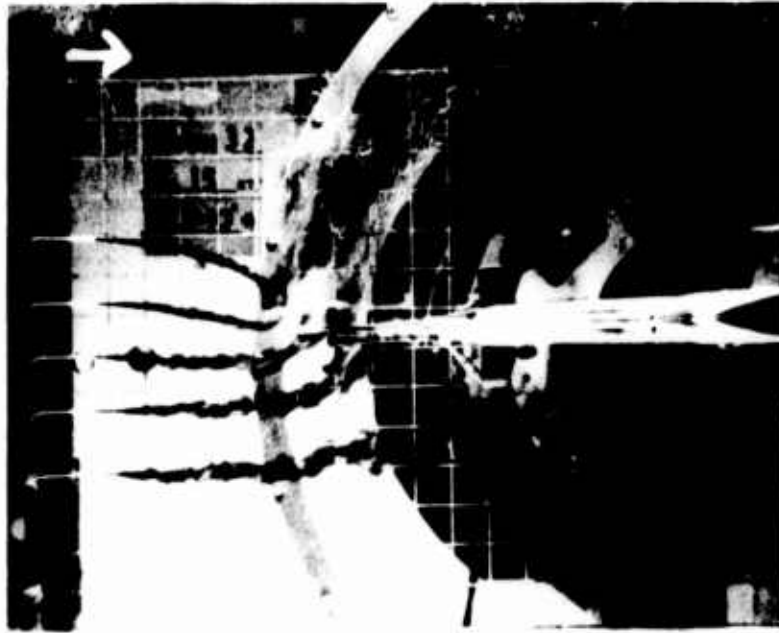
Without Main Rotor



With Main Rotor Operating

Figure 20.   Overhead Observations of Streampath Inflow Pattern
             to the Tail Rotor With and Without Main Rotor.
             Wind Velocity of 15 Knots at a Heading of
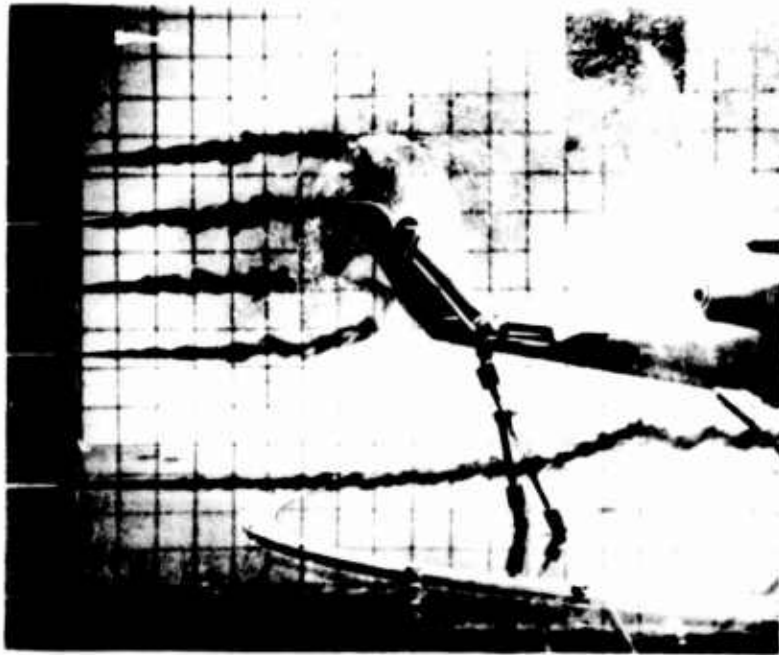             180 Degrees.

Wind Heading of 180 Degrees



Wind Heading of 195 Degrees

Figure 21. Side Observations Illustrating the Variation in
the Inflow Patterns to the Tail Rotor With Main
Rotor Operating for a Wind Velocity of 15 Knots
as the Wind Heading Is Changed.

60
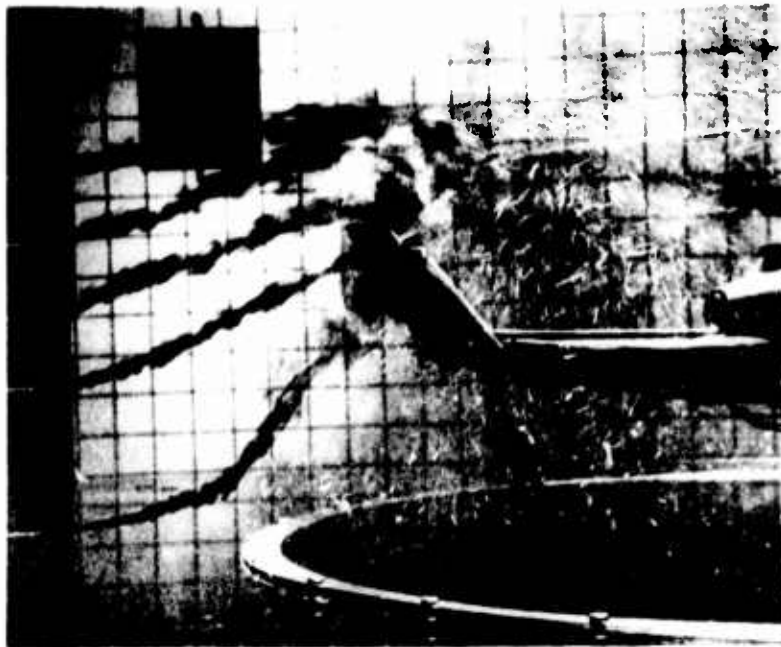
Wind Heading of 210 Degrees



Wind Heading of 225 Degrees

Figure 21.  Continued.

61

Wind Heading of 180 Degrees



Wind Heading of 195 Degrees

Figure 22.   Overhead Observations Illustrating the Variation
in the Inflow Patterns to the Tail Rotor With
Main Rotor Operating for a Wind Velocity of 15
Knots as the Wind Heading Is Changed.

62
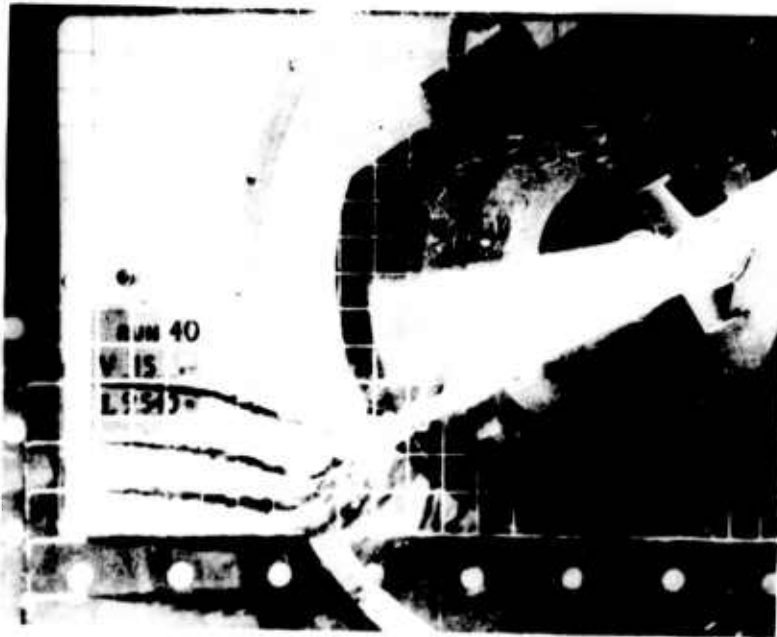
Wind Heading of 210 Degrees
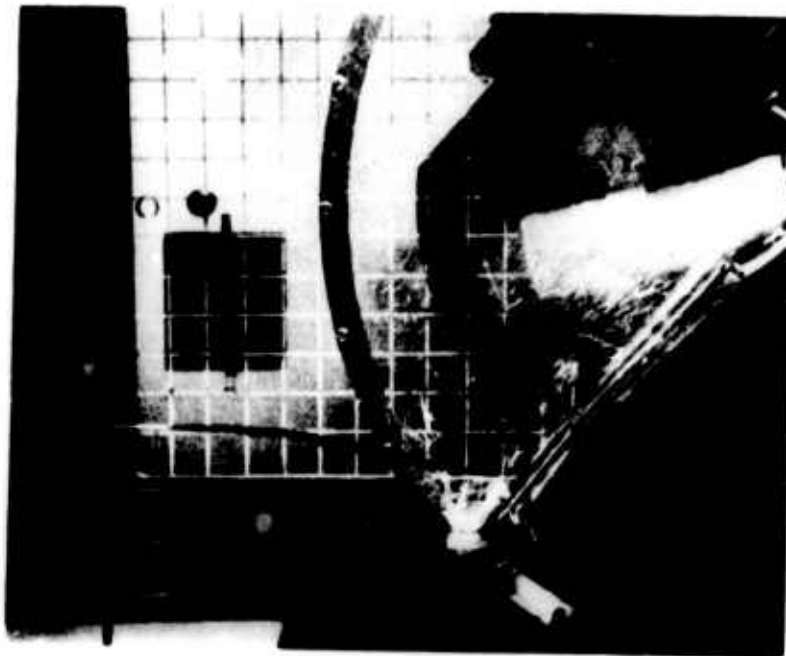


Wind Heading of 225 Degrees

Figure 22.   Continued.

Wind Heading of 180 Degrees
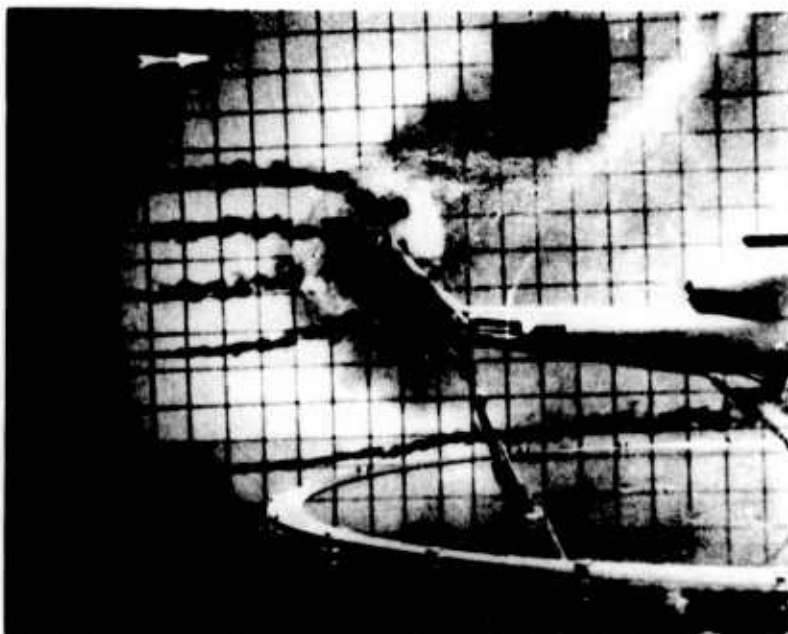


Wind Heading of 195 Degrees

Figure 23. Side Observations Illustrating the Variation in
the Inflow Patterns to the Tail Rotor Without
Main Rotor for a Wind Velocity of 15 Knots as the
Wind Heading Is Changed, (Compare With Figure 21).

64

Wind Heading of 210 Degrees
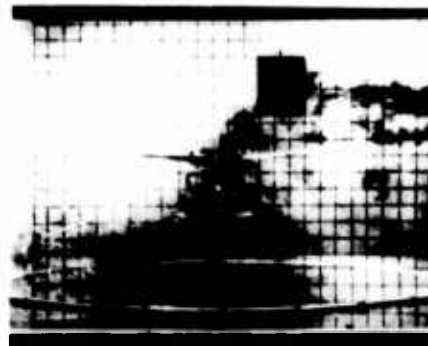


Wind Heading of 225 Degrees

Figure 23. Continued.

65
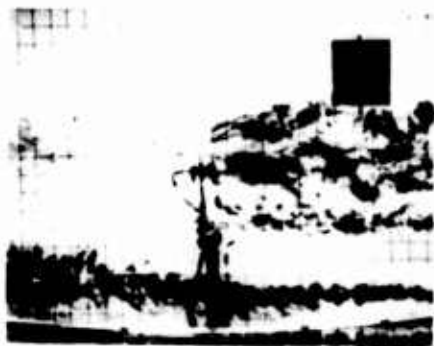
(a)  Velocity 10 Kt

(d)  Velocoty 10 Kt
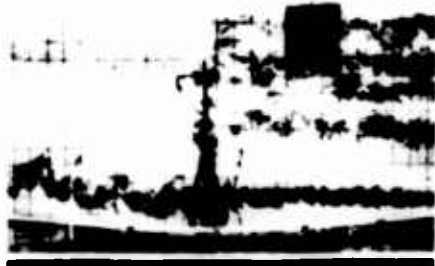


(b)  Velocity 15 Kt

(e)  Velocity 15 Kt
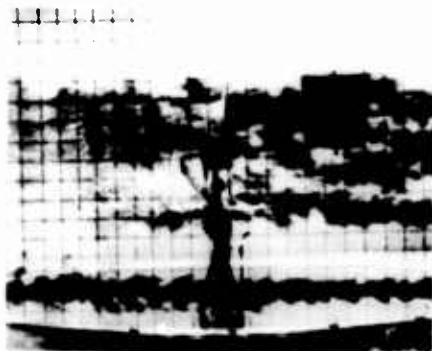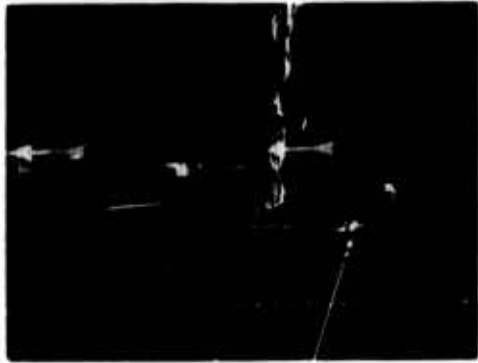


(c)  Velocity 25 Kt

(f)  Velocity 25 Kt

Series a, b, and c Without
Main Rotor

Series d, e, and f With
Main Rotor Operating

Figure 24.   Side Observations of the Inflow and Wake Patterns
With and Without the Main Rotor for Different
Wind Velocities at a Wind Heading of 90 Degrees.

66

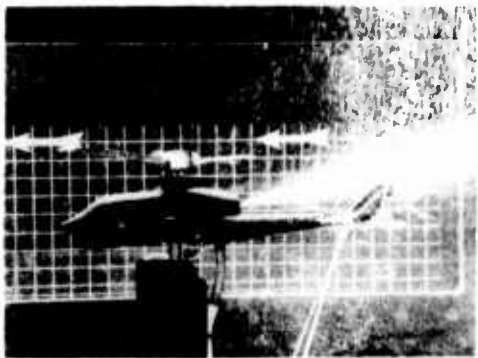Equivalent Jet Velocity
62 fps



Equivalent Jet Velocity
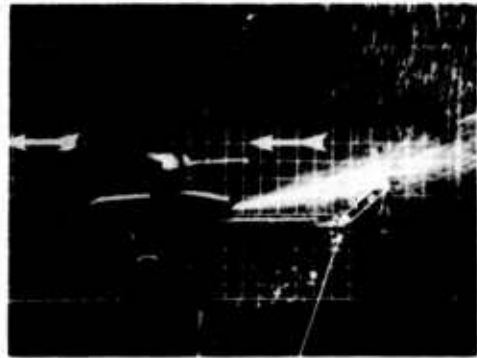70 fps



Equivalent Jet Velocity
112 fps

NOT REPRODUCIBLE



Equivalent Jet Velocity
184 fps



Equivalent Jet Velocity
266 fps
(Actual Operating Condition)



Equivalent Jet Velocity
290 fps

Series (a) Main and Tail Rotors Not Operating

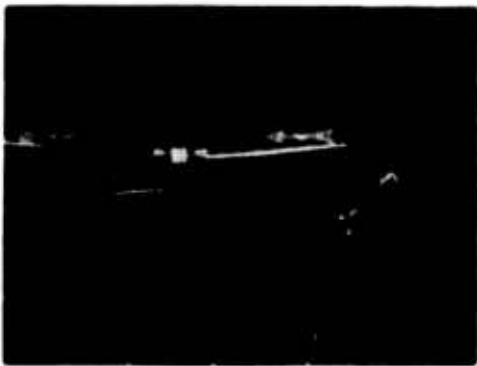Figure 25.  Engine Exhaust Studies With No Wind.

67

Equivalent Jet Velocity
62 fps

Equivalent Jet Velocity
70 fps

Equivalent Jet Velocity
112 fps

Equivalent Jet Velocity
184 fps

Equivalent Jet Velocity
266 fps
(Actual Operating Condition)

Equivalent Jet Velocity
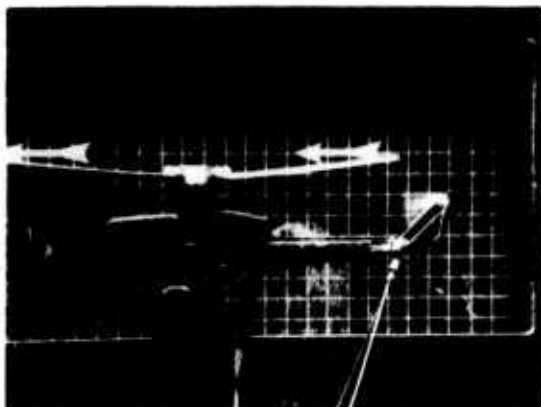290 fps

Series (b)   Main and Tail Rotors Operating

Figure 25.   Continued.

68

Equivalent Jet
Velocity
184 fps

Equivalent Jet
Velocity
266 fps (Full-
Scale Condition)

Equivalent Jet
Velocity
290 fps

Series (a)   Wind Velocity 10 Kt

Figure 26.   Engine Exhaust Studies With Main and Tail Rotors
Operating and a 180-Degree Wind Heading.

69

Equivalent Jet
Velocity
184 fps

Equivalent Jet
Velocity
266 fps (Full-
Scale Condition)

Equivalent Jet
Velocity
290 fps

Series (b) Wind Velocity 20 Kt

Figure 26.   Continued.
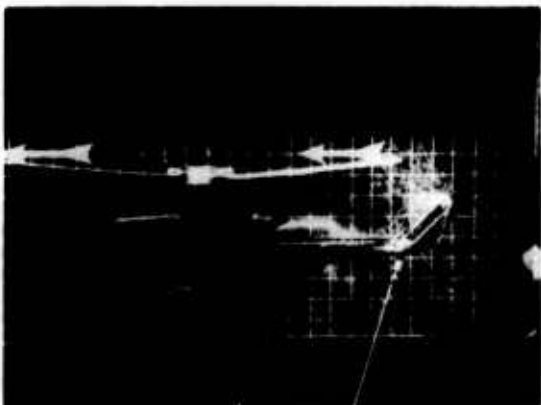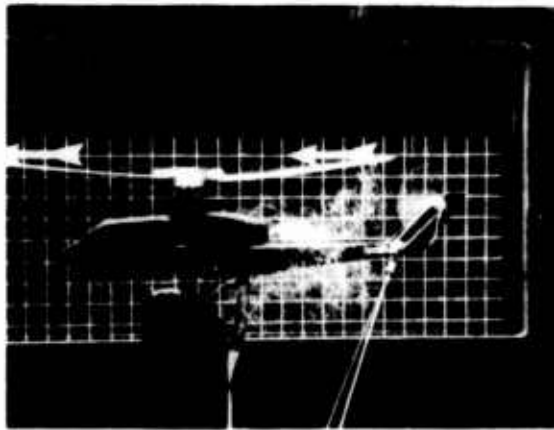
Equivalent Jet
Velocity
184 fps



Equivalent Jet
Velocity
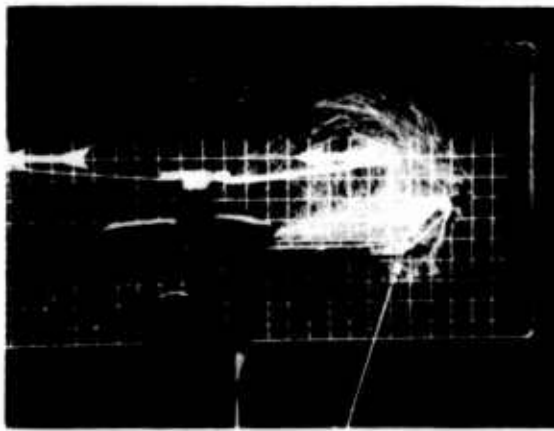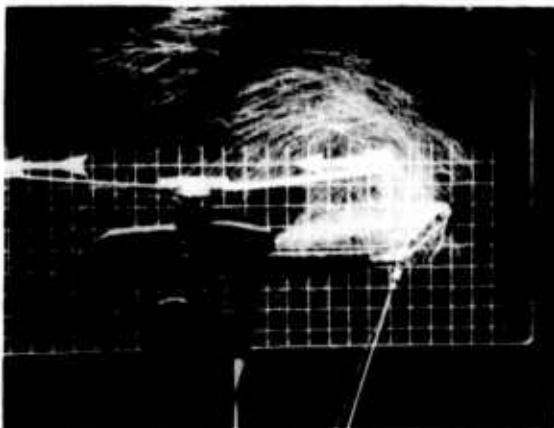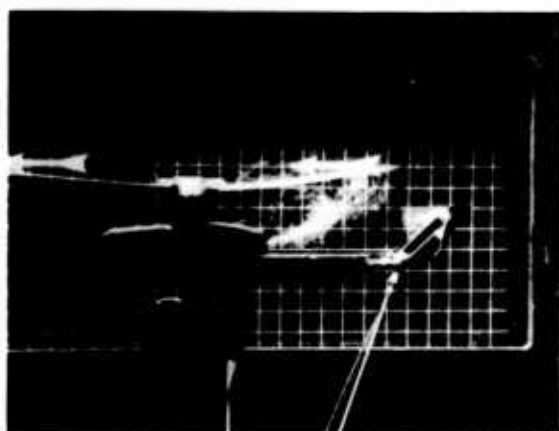266 fps (Full-
Scale Condition)



Equivalent Jet
Velocity
290 fps

Series (c)   Wind Velocity 30 Kt
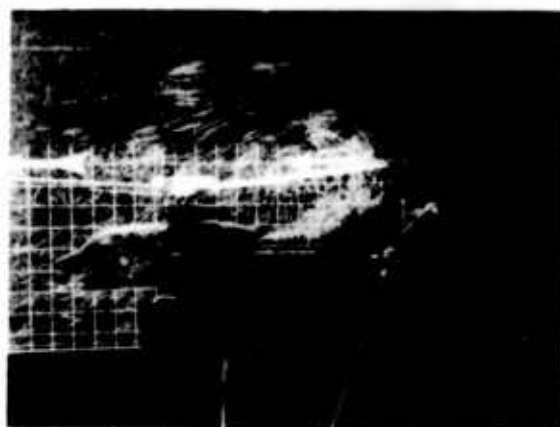
Figure 26.   Continued.

# APPENDIX I

## COMPARISON OF ROTOR LIFT AT TWO REYNOLDS NUMBERS

The necessity for Reynolds number scaling is a well recognized requirement for the performance of meaningful model studies. Using simple strip theory, it is shown in Table V that the vertical lift developed by a hovering rotor operating at a Reynolds number corresponding to flight conditions differs by less than 2 percent from that produced when the rotor is operating at a Reynolds number corresponding to the present model tests performed in a water tunnel.

The ability to closely match the total rotor lift while operating at two widely different Reynolds numbers lies in the fact that below the stall, blade lifting characteristics are virtually independent of Reynolds number, and Reynolds number serves mainly to limit the maximum lift that can be achieved at any radial section. For a helicopter rotor operating at a full-scale Reynolds number all sections are likely to be operating below the stall, while for operation at model-scale some sections may have stalled out. However, if at model-scale only the inboard sections are stalled, the effect on the overall lift will be small since the inboard sections contribute little to the overall lift whether they are stalled or not. Consequently, if model tests are carried out at Reynolds numbers for which only the inboard sections are stalled, such tests will still give good predictions of full-scale total lift, and that is the situation maintained in the water tunnel investigations.

The situation presented in Table V is for a 44-foot-diameter AH-1G rotor having a chord of 27 inches and an NACA 0012 airfoil. The twist in the rotor blade is 0.454 degree per foot. The collective pitch angle is 13.3 degrees. The tip speed of the rotor is assumed to be a constant 800 feet per second. Incompressible flow has been assumed for this comparison, a valid assumption since the comparison is limited solely to an examination of the influence of Reynolds number on total rotor lift. Compressibility effects are likely to be important for determining the true total rotor lift and in the model studies, the incompressible lift values were adjusted to compressible values through the use of the Prandtl-Glauert factor.

TABLE V.  COMPARISON OF CALCULATED TOTAL ROTOR LIFT AT TWO REYNOLDS NUMBERS; HOVER CONDITION; 44-FOOT-DIAMETER ROTOR; 800 FEET PER SECOND TIP SPEED; INCOMPRESSIBLE FLOW ASSUMED; AIR DENSITY OF 0.00218 SLUG PER CUBIC FOOT

| Section | Section Radius (ft) | Section Velocity (fps) | Section Velocity$^2$ (x$10^{-3}$) | Section Angle (deg) | $R_e$ (tip) = 10.3 x $10^6$ | | | $R_e$ (tip) = 1.7 x $10^5$ | | |
|---|---|---|---|---|---|---|---|---|---|---|
| | | | | | Section $R_e$ | Section $C_L$ | Section Lift (lb) | Section $R_e$ | Section $C_L$ | Section Lift (lb) |
| 1 | 1.1 | 40 | 1.6 | 12.8 | Hub | Hub | – | Hub | Hub | – |
| 2 | 3.3 | 120 | 14.4 | 11.8 | 1.54x$10^6$ | 1.185 | 80.2 | 2.55x$10^4$ | .750 | 51.0 |
| 3 | 5.5 | 200 | 40.0 | 10.8 | 2.57x$10^6$ | 1.130 | 212.9 | 4.25x$10^4$ | .785 | 148.0 |
| 4 | 7.7 | 280 | 78.4 | 9.8 | 3.60x$10^6$ | 1.030 | 380.7 | 5.95x$10^4$ | .805 | 297.5 |
| 5 | 9.9 | 360 | 129.6 | 8.8 | 4.63x$10^6$ | .930 | 567.8 | 7.65x$10^4$ | .810 | 494.5 |
| 6 | 12.1 | 440 | 193.6 | 7.8 | 5.66x$10^5$ | .825 | 752.9 | 9.35x$10^4$ | .795 | 725.2 |
| 7 | 14.3 | 520 | 270.4 | 6.8 | 6.69x$10^5$ | .715 | 911.3 | 1.10x$10^5$ | .715 | 911.3 |
| 8 | 16.5 | 600 | 360.0 | 5.8 | 7.72x$10^6$ | .615 | 1043.5 | 1.27x$10^5$ | .615 | 1043.5 |
| 9 | 18.7 | 680 | 462.4 | 4.8 | 8.75x$10^6$ | .505 | 1100.4 | 1.45x$10^5$ | .540 | 1177.0 |
| 10 | 20.9 | 760 | 577.6 | 3.8 | 9.78x$10^6$ | .400 | 1089.0 | 1.61x$10^5$ | .450 | 1224.6 |

$\Sigma$=6138.7 lb

$\Sigma$=6072.6 lb

Difference = 1.01 percent

73

## APPENDIX II

### JET ENGINE EXHAUST SIMILITUDE

Several different approaches were examined before establishing the scaling parameter employed in these studies. Details of the approach selected are presented below:

Nomenclature:

Full-Scale Vehicle: Subscript F     Model: Subscript m

$A_j$ = area of jet exit

$K_T$ = thrust coefficient = $\dfrac{T}{\rho n^2 d^4}$

$T$ = rotor thrust

$V_j$ = jet velocity

$V_o$ = ambient velocity

$d$ = rotor diameter

$n$ = rotor rps

$t$ = temperature

$\rho_j$ = density of jet exhaust

$\rho_o$ = density of ambient air

Values Employed:

Full Scale:

$A_j$ = 203 sq in.

$V_j$ = 266 fps

$d$ = 44 ft

$t$ = ambient 90°F = 550°R
jet exhaust at exit = 1000°R
jet exhaust at tail = 660°R

74

Model:

$$A_j = 0.143 \text{ sq in.}$$

$$d = 14 \text{ in.}$$

$$\rho_j = \rho_o = 62.4 \text{ lb per cu ft}$$

Details of Approach:

Keep the ratio $\left[ \dfrac{\text{Total Momentum of Jet Exhaust}}{\text{Thrust of Tail Rotor}} = \text{Constant} \right]$

for the model and full-scale condition:

$$\left[ \frac{(\rho A V^2)_{jet}}{T} \right]_m = \left[ \frac{(\rho A V^2)_{jet}}{T} \right]_F \tag{1}$$

In general, $T = K_T \rho d^4 n^2$,

$$\left[ \frac{(\rho A V^2)_{jet}}{K_T \rho d^4 n^2} \right]_m = \left[ \frac{(\rho A V^2)_{jet}}{K_T \rho d^4 n^2} \right]_F \tag{2}$$

Assume that $K_T$ of the model tail rotor is equal to the $K_T$ of the full-scale tail rotor,

$$\left[ \frac{V_{j_m}}{V_{j_F}} \right]^2 = \frac{A_F}{A_m} \times \left[ \frac{d_m}{d_F} \right]^4 \times \left[ \frac{n_m}{n_F} \right]^2 \times \frac{\left[ \rho_j \big/ \rho_{amb} \right]_F}{\left[ \rho_j \big/ \rho_{amb} \right]_m} \tag{3}$$

The area ratios and diameter ratios are controlled by geometric scaling, which is 37.1:1.

The n ratio is established by:

    (1)   Main-rotor to tail-rotor gearing ratios the same in the model as in full scale.

    (2)   A full-scale main-rotor tip speed of 800 fps.

    (3)   A model-rotor n of 8 rps

75

$$\frac{n_m}{n_F} = \frac{8 \text{ rps}}{\dfrac{800 \text{ fps}}{22 \text{ ft} \times 2\pi}} = \frac{8}{5.79}$$

Thus substituting in (3) with $\left[\dfrac{\rho_j}{\rho_{amb}}\right]_m = 1$,

$$\left[\frac{V_{j_m}}{V_{j_F}}\right]^2 = (37.7)^2 \left[\frac{1}{37.7}\right]^4 \times \left[\frac{8}{5.79}\right]^2 \times \left[\frac{\rho_j}{\rho_{amb}}\right]_F$$

$$\left[\frac{V_{j_m}}{266}\right]^2 = \left[\frac{1}{37.7}\right]^2 \times \left[\frac{8}{5.79}\right]^2 \times \left[\frac{\rho_j}{\rho_{amb}}\right]_F$$

$$V_{j_m} = \left[\frac{266 \times 8}{37.7 \times 5.79}\right] \times \left[\frac{\rho_j}{\rho_{amb}}\right]_F = 9.75 \left[\frac{\rho_j}{\rho_{amb}}\right]_F^{1/2} \text{ fps} \qquad (4)$$

If the exhaust density were the same as the ambient density,

$\left[\dfrac{\rho_j}{\rho_{amb}}\right]_F = 1$; then substituting in (4)

$$V_m = 9.75 \text{ fps}$$

but the average exit temperature from the nozzle (hot exhaust mixed with cold ejector-nozzle air) is of the order of t = 1000°R.

Therefore, assuming a 90°F day,

$$\left[\frac{\rho_{jet}}{\rho_{amb}}\right]_F = \frac{t_{amb}}{t_{jet}}_F = \frac{550°R}{1000°R} = 0.55$$

76

and substituting in (4)

$$V_m = 9.75 \ \sqrt{0.55} = 7.2 \text{ fps}$$

This is the value employed in these studies.